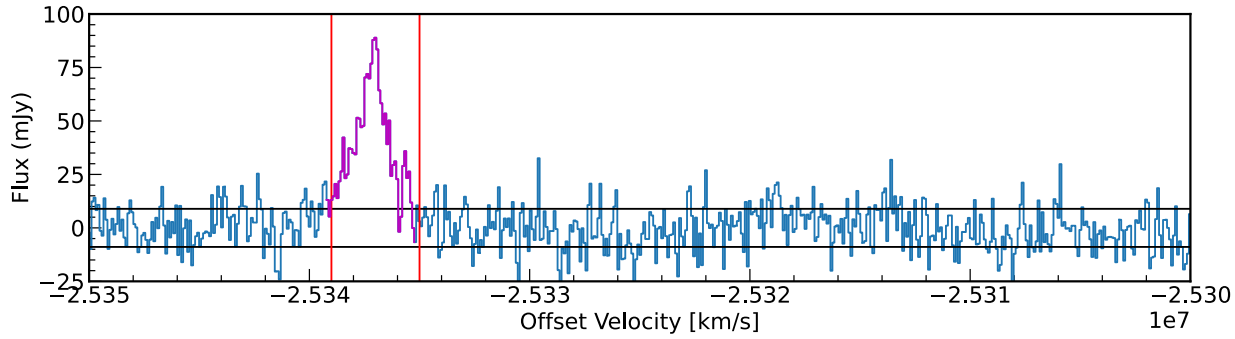

Figure 6.8 *The spectra of the central pixel isolating the $C^{17}O$ J=2-1 emission line towards V1057 Cyg. The black horizontal lines show the calculated ± RMS and the red lines and highlighted magenta line show the frequency range in which the integrated flux is calculated for the final column density calculation.*

relate the transition's column density to the total $C^{17}O$ column density:

$$N_T = \frac{N_u}{g_u} Q(T_{rot}) [e^{-E_u/kT}]^{-1} \tag{6.8}$$

where g_u is a statistical weight unique to $C^{17}O$, $Q(T_{rot})$ is the partition function, and E_u is the upper state energy of the J=2-1 transition. All of these constants are found in the JPL line catalogue (Pickett et al., 1998). See Mangum & Shirley (2015) for an example on how to calculate column densities, with a $C^{17}O$ example listed in their appendix. Once the total $C^{17}O$ column density is found, we can use the isotope ratios to back out the total CO and then H_2 column density. We use $C^{16}O/C^{18}O$ = 1687 and $CO/H_2 = 10^{-4}$ (Bergin & Williams, 2017). Once the H_2 column density is derived per pixel, we sum over the surface area of a set of given pixels to produce a total mass. By eye, we define a "disk" region and a "cloud" region. The disk region is meant to encapsulate the highest central density region, while cloud contains all or most of the high confidence emission. Examples of the $S_\nu \Delta\nu$, N_u, and N_T with the "disk" and "cloud" regions marked for V1057 Cyg are shown in Figure 6.9.

The average $C^{17}O$ column densities, mass column densities, and final "cloud" and "disk" masses are shown in Table 6.3. The "cloud" and "disk" regions are shown in Figure 6.10 with corresponding size scales in au. The Keplarian disk is not resolved in any of our sources, thus "disk" mass should represent an upper limit on the mass available in the protoplanetary disk. The most massive disk, and an outlier in this sample of five sources is V1057 Cyg. Its stellar luminosity and outburst date are otherwise normal compared to the rest of this sample. This source is also, by far, the most line-rich.

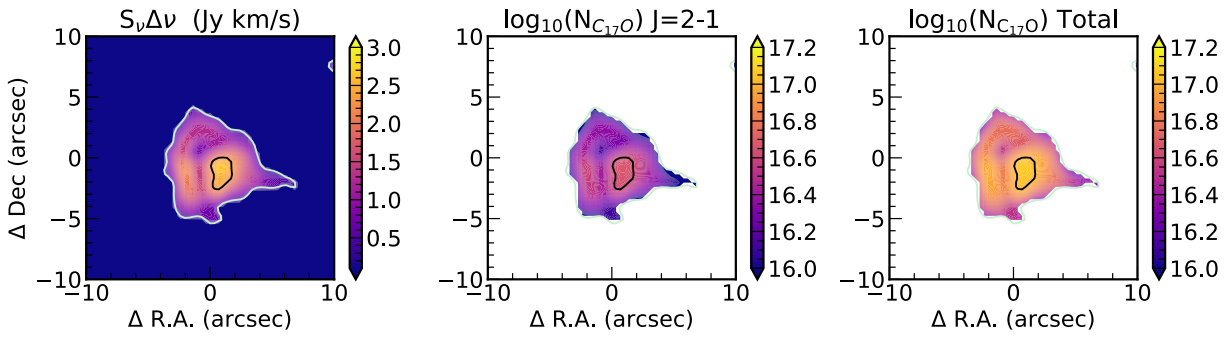

Figure 6.9 *The integrated flux, column density of J=2 level, and total $C^{17}O$ for V1057 Cyg. The black contour indicates an identified "disk" region and the white contour indicates "cloud"*

Table 6.3. Column Densities and Mass

Name	$\log_{10}(N_{C17O}\ [\frac{mol}{cm^2}])^a$	$\log_{10}(N_{H2})\ [\frac{g}{cm^2}])^a$	"Cloud" Mass [$M_\odot$]	"Disk" Mass [$M_\odot$]
V1057 Cyg	16.7	0.47	16.3	1.97
V1735 Cyg	15.6	-0.66	1.36	0.06
V1647 Ori	16.0	-0.20	5.36	0.26
V1515 Cyg	16.2	-0.02	0.79	0.28
V2492 Cyg	17.4	1.2	8.23	0.708

Note. — [a]Here we quote the average over the whole source

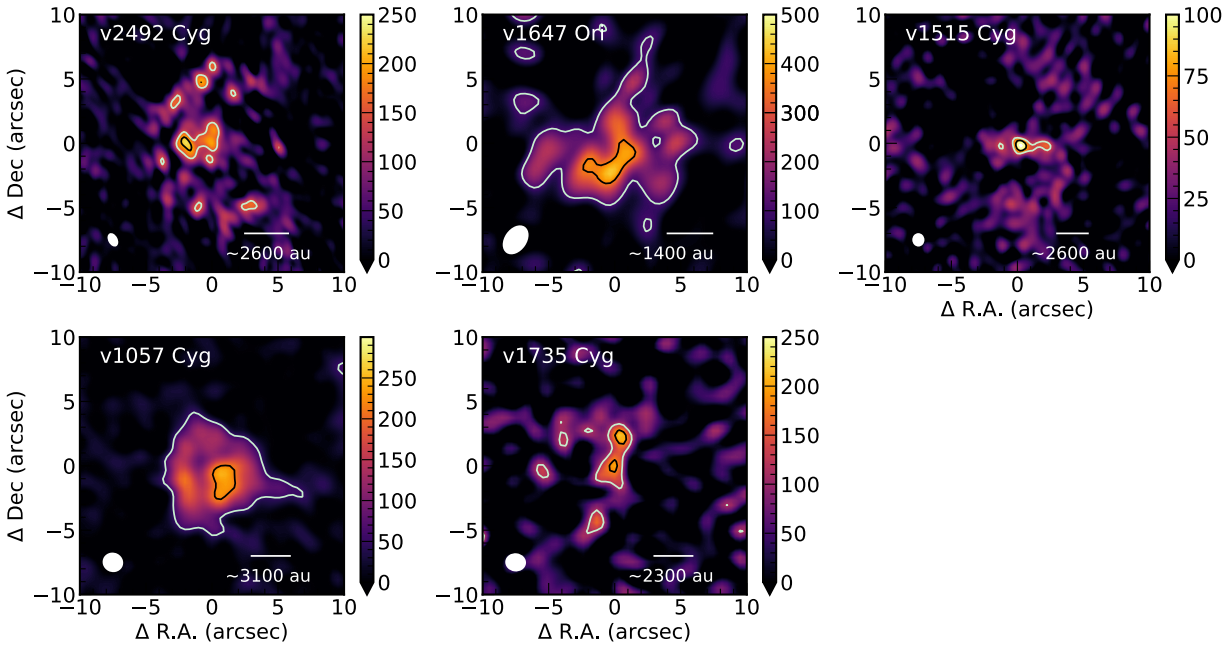

Figure 6.10 *Moment zero maps of $C^{17}O$ with the white contour indicated where "cloud" emission is contained and the black contour is what is considered "disk" emission. The corresponding masses of each region is shown in Table 6.3*

6.3.4 Chemical Composition

Using the low-velocity resolution in the LSB (202.7 - 210.8 GHz) and the USB (218.2 -226.0 GHz) we identified distinct lines that lay well above the noise level without additional velocity sampling nor additional analysis that could pull out faint lines. Thus the lines identified are bright and confident detections, and there may be fainter lines hiding in the noise.

All sources had successful detections of ^{13}CO, $C^{18}O$, and $C^{17}O$ that were used to determine the mass and structure of each outbursting system. V1057 Cyg had a $^{13}C^{18}O$ detection while none of the other sources did. V1057 Cyg had 24 distinct emission lines beyond the CO lines, with a handful of other tentatively detected faint lines. The strong emission lines came from transitions of CH_3OH, HC_3N, CH_3CN, H_2CO, $H_2{}^{13}CO$, SO, SO_2, OCS, H_2CS, and HDO. There are tentative detections of long complex organic molecules that have also been seen in star-forming regions and young stellar objects including HNCO, H_2CN, CH_3OCHO, CH_3CHO, and H_2CCO. The USB of this source contained the most lines, and this is highlighted in Figure 6.11.

The other four sources contain detections of H_2CO and SO, and V1515 Cyg also has an SO_2 detection. Contrasted to the high-mass V1057 Cyg, these sources are not line rich, and only contain bright molecules that carry oxygen. All emission beyond the CO lines are spatially unresolved, and some can only be clearly seen in the spectra. Some transitions of SO and SO_2 are captured in the

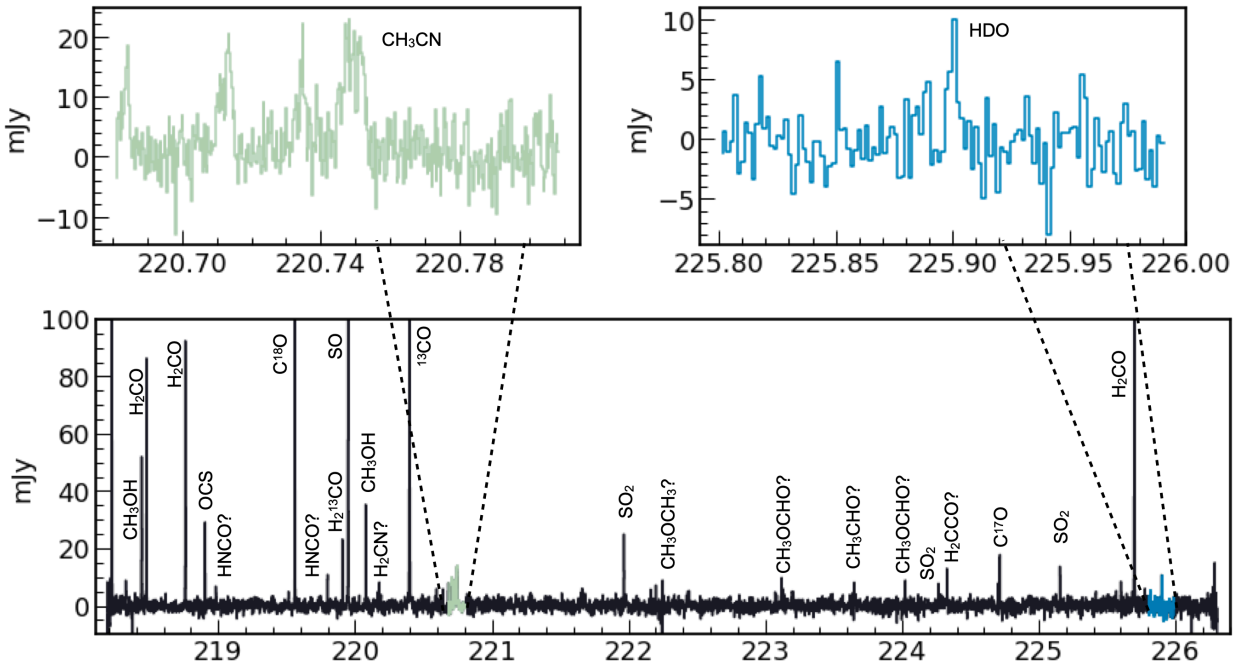

Figure 6.11 *The spectra of the USB towards V1057 Cyg. The CH_3CN and HDO detections are highlighted.*

high-velocity windows, and contain line wings and other non-Gaussian profiles.

6.4 Discussion

Mass is a fundamental property when it comes to understanding the protoplanetary disk environment and FU Ori outburst events. The quickest and most often used technique to extract disk masses is dust thermal continuum observations. Assuming optically thin dust emission and a gas-to-dust ratio, a gas mass can be calculated from the dust observations. To compare this method versus a mass extraction from an optically thin gas-tracer, we compare gas mass values derived from the continuum and $C^{17}O$ J=2-1 flux from our sample, as well as masses derived from another survey that used $C^{18}O$ J=1-0. A comparison between the derived total gas mass from $C^{17}O$ emission versus that from continuum flux and $C^{18}O$ J=1-0 are shown in Figure B.9. The derived masses from $C^{17}O$ J=2-1 are on par with those derived from $C^{18}O$ J=1-0 (Fehér et al., 2017) with a V1057 Cyg as an outlier. The quoted $C^{18}O$ masses were measured for observed "clumps" a few thousand au wide in each source, so comparable to our "disk" mass. Those observations were made with the Plateau de Bure Interferometer and 30m IRAM telescope, thus those observations are more sensitive to large scale structure and have a larger overall beam. In Figure B.9, we see that for the four sources in the Fehér et al. (2017) survey, our $C^{17}O$-based masses result in higher

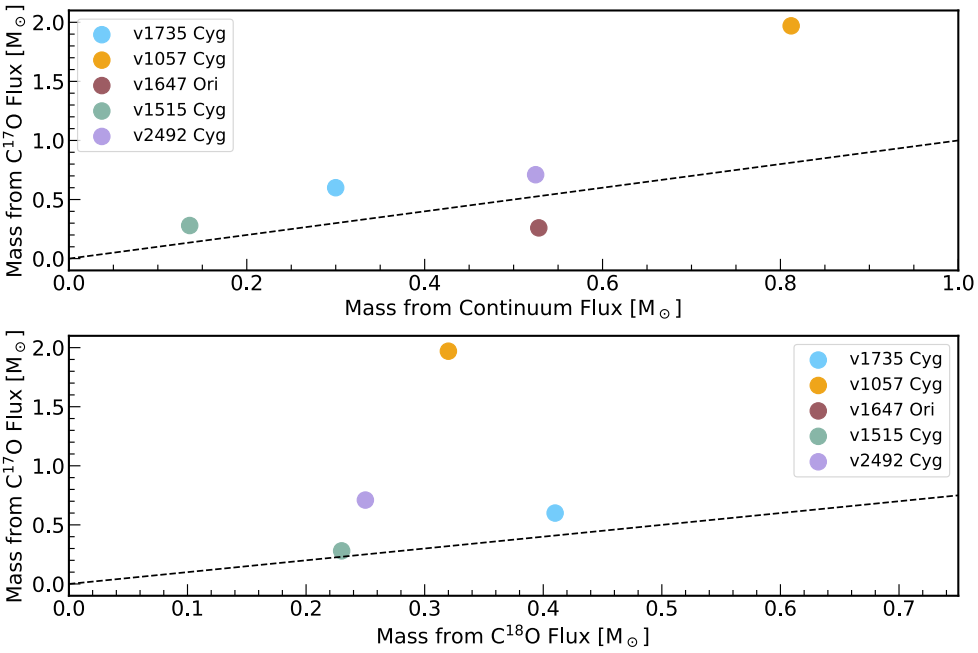

Figure 6.12 *The derived masses for the central clump in each source using our NOEMA observations of $C^{17}O$ and continuum (top) and $C^{18}O$ J=1-0 from Fehér et al. (2017).*

gas masses. This is to be expected if the $C^{18}O$ J=1-0 emission was more optically thick than $C^{17}O$ J=2-1. It is worth noting, however, that the exact emission areas between surveys may differ. We find V1057 Cyg to be significantly more massive than its FU Ori counterparts and its $C^{18}O$ mass. In our continuum observations, there appear to be two central maxima corresponding to V1057 Cyg being a binary system and it has previously been identified as a tentative binary system. No other source in our sample is a confirmed binary system, although that cannot be ruled out. Other than than, V1057 Cyg appears to be comparable or average to our other four sources in terms of its bolometric luminosity, local temperature, stellar type, time since outburst, and continuum mass.

In Figure B.9 we also compare our $C^{17}O$-derived disk gas mass to that estimated from the dust continuum. The mass derived from the continuum correlates with our derived $C^{17}O$ mass. V1057 Cyg and V1647 Ori stick out as outliers, with V1057 cyg having a higher $C^{17}O$ derived total gas mass than from the continuum and V1647 Ori being lower mass. The continuum emission from V1647 Ori stands out as the brightest in our sample, and the peak of that intensity corresponds to a dip in $C^{17}O$ emission, suggesting that the continuum there is optically thick, and is blocking out some $C^{17}O$ emission, thus producing a lower gas mass than is actually present. V1057 Cyg sticks out again is being more massive than would have been assumed than just continuum flux, and a gas to dust ratio of ≈200-300 would be needed to reproduce the mass from $C^{17}O$. The other possibility is that the continuum from V1057 Cyg is optically thick, or has large grains that hold most of the mass which is invisible to these observations.

Our most massive source, V1057 Cyg, is also the most molecule-rich. It appears to have released the molecular complexity that is expected in the ice, and these sublimated ices have remained in the gas perhaps since its outburst in 1970. Although we have not derived chemical abundances, based on the detected molecular lines the composition appears similar to that of the volatile content on the grains sublimated into the gas-phase keeping the expected level of molecular complexity. This is very similar to another outbursting source: V883 Ori. V883 Ori has been extensively observed with ALMA and has successful detections of COMs, HDO and $H_2^{18}O$. It would be insightful to also observe V1057 Cyg with the sensitivity of ALMA, overlapping with the observed lines in V883 Ori. V883 Ori does not have as much envelope structure as V1057 Cyg, thus represents a slightly more evolved system. Comparing the molecular complexity in these two sources would shed light onto how volatile chemistry evolves.

All other sources only had H_2CO and SO detections. These molecules are commonly seen in disks and young stellar objects. H_2CO is one of the most abundant COMs seen in the gas, although it is expected that CH_3OH is the most common COM when considering the ice and gas reservoir combined, so it is surprising that there were no detections of CH_3OH in these four other sources. This suggests that the ice reservoir has frozen back onto grains in the time since the original outburst. Using Equation 1 in Visser et al. (2015), an assumed freeze-out temperature of 50 K and 50 years post-outburst, the number density of the medium is required to be $\approx 10^8$ cm^{-3}. SO is usually a warm gas-tracer, or shock tracer. The SO emission is unresolved, so it is impossible to disentangle the emission from a disk or an outflow. With such a limited series of molecular complexity in very warm systems, this poses more questions. Did the initial outburst shock or warm up the surrounding medium to a level in which COMs were broken apart, and a reset-chemistry remains today? Or were these molecules removed from the gas in another way? They could be frozen out in deeper layers that have cooled off over time, or chemically removed. If the majority of FU Ori-type outbursts result in a 'reset' chemistry that would have a profound impact on our understanding of the chemical environment in which planets and small bodies are formed in.

These question cannot be answered with this data, and requires follow up. The fact that most of these outbursting sources did not show a level of chemical complexity that is seen in V883 Ori or V1057 Cyg was not expected. A wider survey of these sources, probing the masses and chemical inventory could shed light on the process that is impacting this chemistry and how common it might be. NOEMA has proven to be a powerful tool to conduct such a survey, and the SMA offers similar observing capabilities and probes more of the southern sky as well.

6.5 Conclusion

Using the NOEMA interferometer, we observed five outbursting sources, three FU Ori objects and two EX Ori/Peculiar sources. $C^{17}O$ was detected in each source and was found to be optically thin, thus a mass tracer. We found masses of the centrally peaked clumps from 0.06-1.97 $M_\odot$ and "cloud" masses of 0.79-16.3 $M_\odot$. A molecular inventory of each source was taken, and it was found that V1057 Cyg was uniquely molecularly rich, with long COMs, four different sulfur-bearing molecules, and a water detection. The other four sources only had H_2CO, SO, and SO_2 detections in addition to the CO. This could suggest a reset-chemistry in certain out-bursting environments. More follow-up observations and modeling should be done to explain this pattern.

CHAPTER 7

Conclusions and Future Work

This thesis is motivated by characterization of protoplanetary disks using the high resolution observations and thermo-chemical modeling. Producing 2D thermo-chemical models that reproduce multiple observations originating from distinct regions of the disk was not trivial. However, when implemented successfully, proved to be powerful. In Chapter 2, along with an HD flux, the mass of the disk around TW Hya was constrained and the strong degeneracy between CO flux and disk mass was shown. In Chapter 3, using the same technique of reproducing radial profiles of CO and its isotopologues, our model already well-reproduced the 2D emitting heights derived by direct observations. This suggests that our initial assumption on the density distribution, and reproducing radial profiles from ^{12}CO through C^{17}O gives a valid 2D simulation of the disk. Chapter 4 used the models derived from Chapters 2 and 3 to provide a solution to an open question in the field. I showed that by relying on the likely effects of dust evolution, the high flux we see from CH_3CN can be explained naturally when a slight increase in the UV flux in the densest parts of the disk. Chapter 5 moved away from large-scale 2D thermo-chemical reproductions, and was a purely theoretical exploration of the impacts on water UV-shielding and excess chemical heating on the $H_2O/H_2^{18}O$ ratio, and their resultant spectra. This will motivate future JWST work. In Chapter 6, I present new observations of five FU Ori objects, revealing their ice and gas chemistry as well as their masses using the optically thin tracer C^{17}O. All together, these chapters motivate the use of 2D thermo-chemical models to gain a detailed understand of the planet-forming environment.

In the near future, direct connections between planets and their birth environments will be possible. JWST is set to spend $>$500 hours characterizing exoplanet atmospheres and protoplanetary inner-disks. Lines detectable by JWST will primarily emit from the upper atmosphere of the disk, while terrestrial planets and hot Jupiters are likely accreting material from a coinciding radius, but at the midplane.

The use of 2D thermo-chemical models is necessary to extrapolate JWST observations to the inner disk, and provide that direct connection from planets to their natal conditions. The vast majority of known exoplanets exist within 10 au (See Figure 7.1). Thus, the planet forming zone

extends from <1au out to tens of au. ALMA has been the state-of-the-art instrument for protoplanetary disk characterization, however it is only sensitive to the outer disk, beyond ≈ten au. JWST is required to fill in our knowledge gap. It will probe warmer temperatures, thus material closer to the host star. State-of-the-art models and observations will be necessary in order to create the most highly constrained protoplanetary disk models available, probing all the way down to the planet-forming midplane. This will involve advanced modeling of both JWST and ALMA data, and uniquely will provide insight to the midplane deep within the disk. This thesis has set the field up for success to complete these goals.

7.1 Using the C/O ratio as a Tracer of Planet Formation History

Chemical signatures found in exoplanet atmospheres contain information regarding where they formed within a protoplanetary disk. The C/O ratio is a fantastic formation tracer, as it changes as a function of radius between the gas and ice populations (see Fig. 7.1). At critical snowlines, the C/O ratio will increase or decrease as key carbon and oxygen carrying molecules freeze-out onto grains. Planets form at the midplane and first accrete solid material to form the planetary core, then gaseous material into its atmosphere. Thus, the chemical fingerprint at a specific radial location is inherited into the bulk chemical composition of a given planet. Jupiter exhibits an enhanced C (and N) abundance, and this has suggested that it must have formed beyond the CO and N2 snowlines, or past 30 au(Bosman et al., 2019; Öberg & Wordsworth, 2019). In addition to radial variation, the C/O ratio may also change over time due to chemical and physical evolution in the protoplanetary disk system, adding temporal information encoded into an exoplanet's observed C/O ratio.

To connect a planet's unique chemical signature to a location and time of formation requires advancements from two distinct fields.

1. More exoplanet atmospheres need to have characterized C/O ratios.
2. The C/O ratio need to be spatially mapped out throughout a variety of protoplanetary disks all the way down to the midplane.

Advancement (1) is now possible (Madhusudhan et al., 2011; Zhang et al., 2021c) and is an actively growing field. I will lead the field in Advancement (2). This requires the combination of JWST and ALMA observing capabilities in concert with 2D thermo-chemical modeling.

7.1.1 Unveiling the Inner Disk Environment

The inner disk acts as an influential medium in which stellar radiation must pass through before accessing the outer disk, from which most of our current protoplanetary disk understanding is

derived. The inner disk as we know it hosts a unique physical environment and geometry. How the inner disk physical environment may affect JWST spectra has yet to be explored. A theoretical exploration of the inner disk geometry and host star properties on IR observations is long overdue. With *Spitzer* and optical-based observations, there are predictions for a dust free region, a distinct inner disk scale height, and inner disk radius that is dictated by the mass accretion rate onto the star. It is an open question as to how these regions alone may affect the formation of exoplanets. However, they will have a profound effect on IR spectral features due to how they influence local temperature and emitting areas. Understanding the unique effect or degeneracies that these inner disk physical parameters will have on molecular spectra need to be identified in order to accurately extract 2D thermal structures and chemical distributions.

I propose constructing a grid of 2D thermo-chemical models that span multiple inner disk scale heights, the existence or non-existence of a dust-free zone, and inner radii limits based on observed mass accretion rates for typical JWST sources. For each model, JWST spectra can be simulated focusing on the most frequently observed molecular lines (i.e. H_2O, C_2H_2, CO_2) and a spectral energy distribution. Unique spectral features can be identified that will tell us what the inner disk environment is like. For example, high accreting stars are predicted to have an inner disk edge that is farther away from the star. That distant inner disk boundary will likely result in a brighter mid-IR flux in the spectral energy distribution. The results from this grid of models could be used by the broader community to analyze JWST spectra. With this project, any JWST observer could glean information concerning the inner disk geometry and thermal structure from a JWST spectrum without the need to run time-consuming 2D thermo-chemical codes.

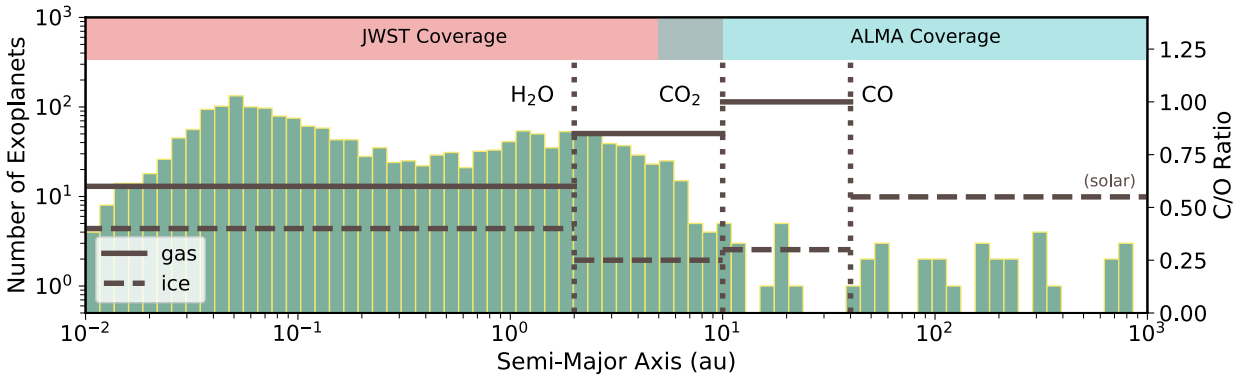

Figure 7.1 *The distribution of semi-major orbital distance across the known exoplanet population in context with the C/O ratio across a typical protoplanetary disk. Overplotted in grey are an example of how the C/O ratio changes through a typical solar-mass protoplanetary disk based on the location of critical snowlines, distinct radial positions where H_2O, CO_2, and CO freeze-out onto grains. C/O data is extrapolated from Figure 1 in Öberg, Murray-Clay & Bergin 2011.*

7.2 Specialized Models of Disks Focused on the Main Planet Forming Zone

To understand the planet-forming zone with high certainty, it is essential to focus on individual disks. Many disks will be widely observed with both ALMA and JWST in dust and molecular lines that probe many overlapping heights and radial extents. Observations from ALMA and JWST need to be considered in tandem so that the full picture of this key planet-forming region is understood. Currently, simple slab models are being used to identify molecular species within the first spectra from JWST. More advanced disk modeling will complement these initial models and utilize their retrieved chemical abundances. A model which reproduces as many of these observations as possible towards a single disk will create a highly constrained chemical and physical environment, and provide an ideal laboratory for exploring the connection between exoplanets and disks. Reproducing multiple observations simultaneously is computationally expensive and requires many rounds of human-driven iteration in order to converge to a solution.

Does the C/O ratio change between the inner and outer disk? Many known exoplanets now exist within 1 au of their host star, but did they form there? To answer that question, we must characterize the C/O ratio within the inner disk throughout a variety of protoplanetary disks. This will be done with JWST. Highly constrained models should be made for the first few disks observed using the new JWST spectra and all available ALMA archival data. This will result in the first-ever 2D maps of the chemical distribution all the way down to the planet-forming midplane that include strong constraints on the inner disk. With JWST spectra, a C/O ratio of the inner disk will be determined. Follow up observations with ALMA of C_2H, CH_3CN, HC_3N will be sought towards all disks with an JWST-constrained inner disk environment and otherwise poorly constrained outer disk environment. These models will show if the inner disk hosts a unique environment, unlike what we have seen in the outer disk, or if the inner and outer parts of the disk are chemically related. Either answer will have a tremendous impact on the chemical signatures imprinted onto forming exoplanets.

Does the C/O ratio evolve over time? Increasingly the Class II protoplanetary disks that have been observed with ALMA tend to exhibit C/O ratios that are above that of the sun and ISM (see Fig. 7.2). When and how the C/O ratio increases within a disk is not well constrained. Bergner et al. (2020) presented a survey of disks including 12 gas-rich evolved dsiks (Class II); half are less than 4 Myrs while the other half are older than 4 Myrs. The survey observed volatile material, including C_2H which is only present in gas with a high C/O ratio. The majority of these disks are slated to be observed with JWST, adding information from the inner disk. I will aim to produce 2D thermochemical models that reproduce the archival C_2H data and future JWST data that traces the C/O ratio in the inner disk (i.e. C_2H_2, CO_2). Trends in the C/O ratio between young and old gas-rich

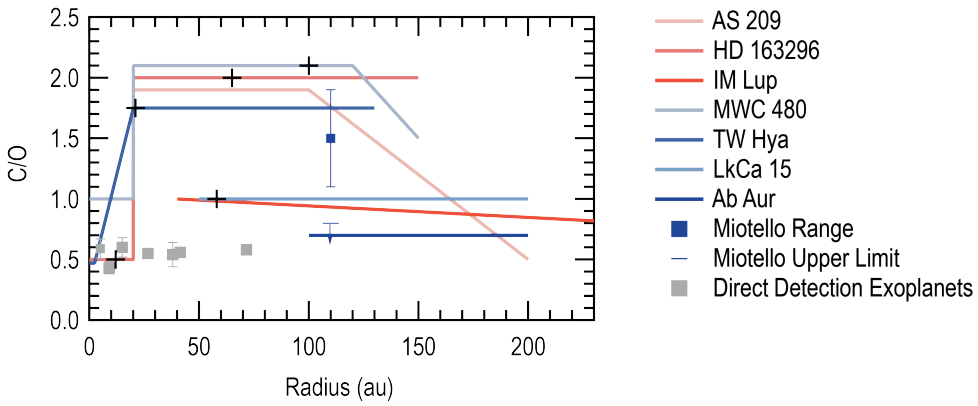

Figure 7.2 *Derived C/O values in disks (lines) and directly imaged exoplanets (points). Image credit: E. Bergin*

disks should be sought out.

7.3 Complex Organic Molecules as a Signpost for High C/O ratios and the Late-stages of Planet Formation

My previous work presents a major breakthrough in the way we look at the chemical environment present during the final stages of planet formation. I predict UV-enhanced, carbon-rich chemistry present in older gas-rich disks. However, this hypothesis is built upon measurements of only two disks, and the Molecules with ALMA at Planet Forming Scales survey represents the largest sample of disks with COMs emission. This survey contains five disks, which present a biased sample, as they are some of the brightest and most massive disks. I propose to prove or disprove this theory, and constrain its effect on final chemical signatures. This can be addressed in two radio observation based projects.

CH_3CN and HC_3N have been the targets of recent ALMA programs towards planet-forming disks, and their emission can be used to trace the C/O ratio near the midplane and inner disk. Within the $\approx$10 disks that have been targeted so far, these molecules appear to be common and with emission that is brighter than predicted (e.g. Bergner et al., 2018) and require super-stellar values of C/O (Cleeves et al., 2018; Calahan et al., 2023). Most of the C/O derivations within protoplanetary disks come from the easier-to-observe C_2H, however C_2H primarily probes the atmosphere of the gaseous disk (Bosman et al., 2021c), *not the planet forming midplane nor inner disk.* CH_3CN and HC_3N are seen to emit from denser and cooler regions, much closer to or directly overlapping with these key planet-forming regions (see Fig. 2, Ilee et al., 2021). A broad survey of CH_3CN and HC_3N will constrain the C/O ratio within the midplane and inner disk, and will link

atmospheric C_2H ALMA observations and warm inner disk C/O data from *JWST*.

Second, we should look for more COMs in the disks we believe this carbon-rich chemistry to exist. My thermo-chemical model with a photo-chemical equilibrium in a high C/O environment predicts more COMs to be highly abundant in the gas such as HC_5N, C_3H_3, and C_6H. However, these large COMs have not been targeted towards any protoplanetary disks. The successful detection of COMs that my model predicts would act as a signpost to a unique end-stage chemistry for forming planets.

7.4 Concluding Remarks

The future of the characterization of planetary formation environments is full of potential and many different avenues that need to be explored! We live in time where we can probe down to planet-forming scales in disks 100s of light years away and can observe the terrestrial-planet forming gas to make direct connections to exoplanets using chemistry. Observations alone will not lead to the connections between protoplanetary disks and exoplanets. These high resolution observations need to be interpreted and understood by using disk models. These models eventually need to account for dust evolution, chemistry, and hydrodynamics as each of these will impact forming planets and features and patterns found in observations.

APPENDIX A

TW Hya Mass and Temperature Appendix

A.1 Parameter Effects on Simulated Observations

Through exploration of our model and the parameter space of the properties listed in Table 2.3, we find that CO emission is most strongly affected by gas and small dust parameters. Here we list how the CO integrated intensity profiles respond to changes in parameters. These findings are specific to this TW Hya model, but can be extrapolated to similarly inclined gaseous disks. The following discussion is based off of the model parameter values from Zhang et al. (2019) presented in Figure A.1:

A.1.1 γ : Power-law Index of Surface Density

γ is a power-law index for the surface density (see Equation 2.1) with a maximum value of two. Increasing γ affects the distribution by concentrating the given component (gas, dust) towards the inner disk region, increasing the column density of gas and dust. A decrease in γ results in a more even distribution of the mass component. It has the strongest effect on the emission arising from the inner 25 AU, especially for the rare isotopologues. Altering gamma from 0.75 to 0.9 in both small dust and gas results in very little change in ^{12}CO 2-1 and 3-2, but at least a 10% increase across all C^{18}O lines. In our final model, we increased γ in both the gas and small dust, as they are coupled, from 0.75 to 0.85 which aided in adding to the intensity in the inner 25 AU.

A.1.2 Ψ : Power-law Index For Scale Height

Typical Ψ values are between 1.1 and 1.2 for TW Hya, and affects the scale height over different radii, with an increase in the flaring as Ψ increases. Changes in Ψ down to 0.05 have a significant effect on the final integrated intensity profiles. Generally, lowering Ψ results in an increase in intensity in the inner disk ($<$ 25 AU), and beyond $\approx$ 25 AU features are 'smoothed' ouft. This is due to the increase of gas surface density towards the inner AU when flaring decreases. The

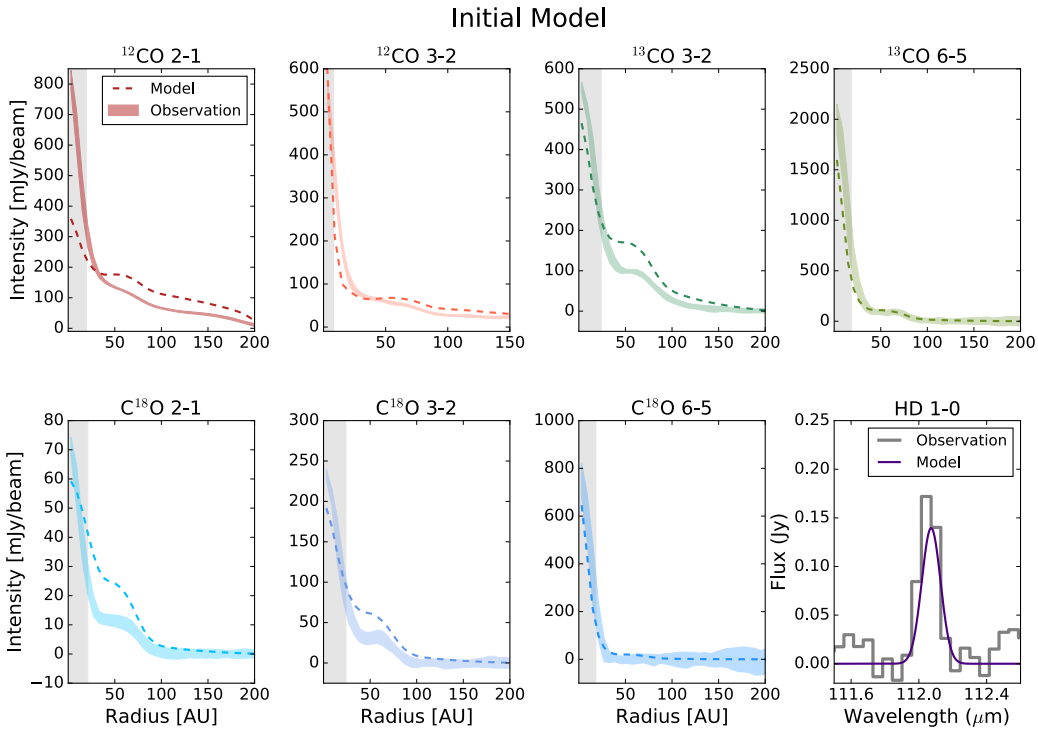

Figure A.1 The integrated line profiles of CO and its isotopologues from ALMA observations (solid lines) and the simulated observations from RAC2D using model parameters from Zhang et al. (2019), and listed in Table 2.3

most extreme value of Ψ we explored was 1.6, and at that point the modeled intensity profiles plummeted down to between 25% of their original flux to zero within 20 AU. Beyond 20 AU, there is emission comparable to the original model. The thermal profile derived from the initial parameters (shown in Table 2.3 and discussed in Section 2.2.3) produced CO lines that were too dim within 25 AU by a factor of 2 in ^{12}CO, ^{13}CO 6-5, C^{18}O 6-5 and $\sim$ 30% in ^{13}CO and C^{18}O 3-2. We find that the only way to significantly brighten the inner regions while simultaneously keeping the intensity in the outer regions low is to allow the gas and small dust to have slightly different Ψ values. The gas component is given a Ψ value of 1.1, while the small dust is given Ψ= 1.2. Due to the fact that our critical radius is beyond the gaseous radius, even though the dust has a higher flaring angle, it lies below the gas. This creates a thin region at the upper layer of the disk where only gas resides; this region has a thickness of $\sim$ 1.2% of a given radius. In this gas-rich layer, CO and HD lines become brighter, noticeably within the inner few AU. There are no other parameters that we explored that accomplished this, the closest being γ, which increases emission within 50 AU, but smooths out the feature beyond 50 AU.

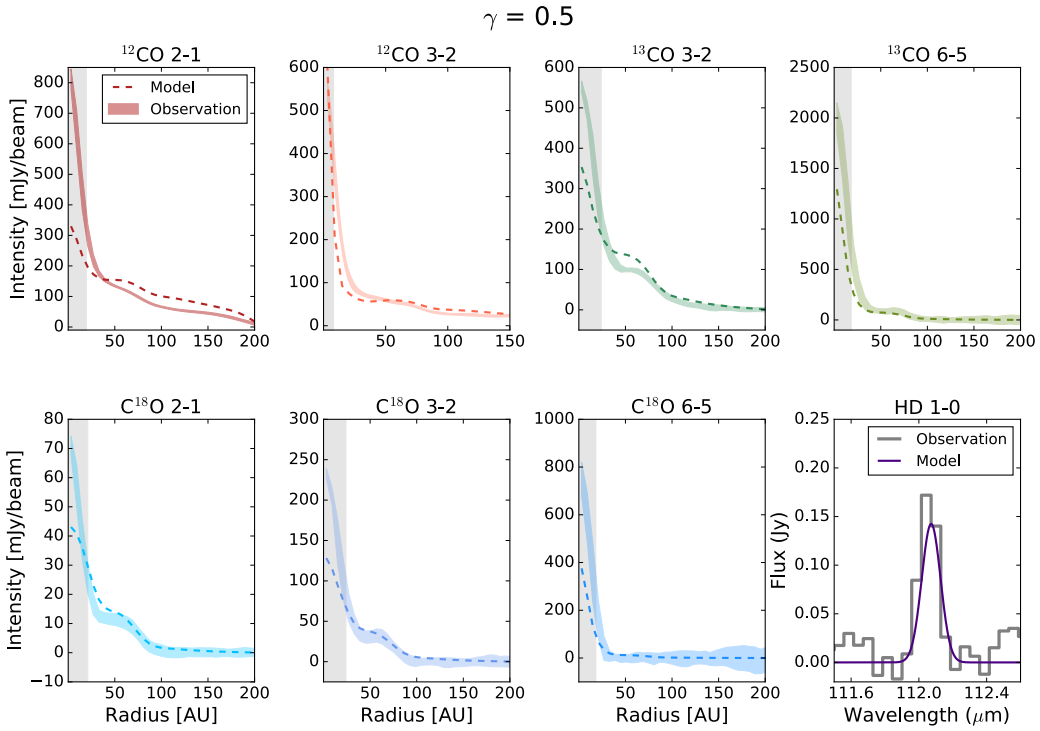

Figure A.2 The integrated intensity profiles of observations and a model based of the initial model (A.1) but with γ in the gas and small dust = 0.5.

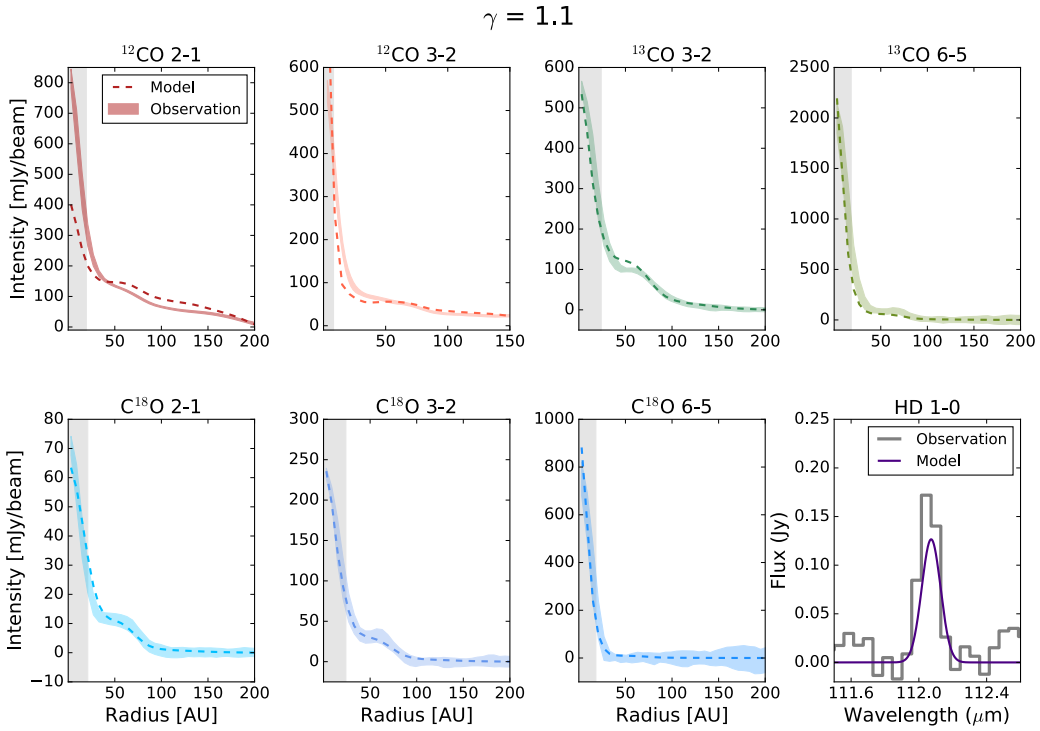

Figure A.3 The integrated intensity profiles of observations and a model based of the initial model (A.1) but with γ in the gas and small dust = 1.1.

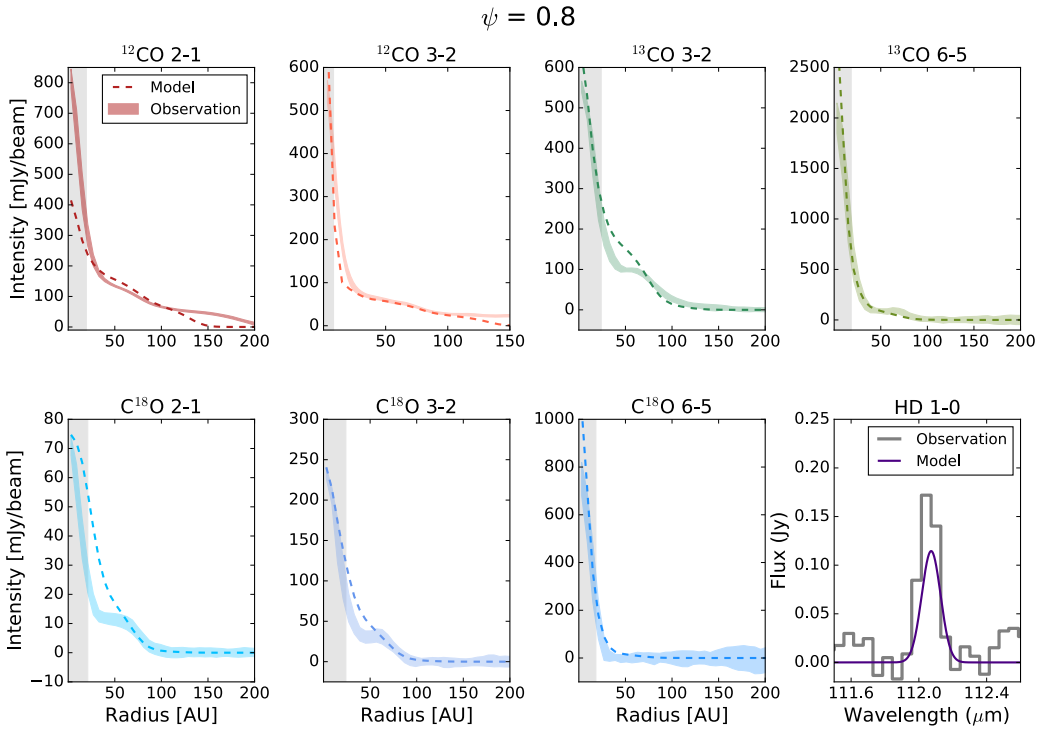

Figure A.4 The integrated intensity profiles of observations and a model based of the initial model (A.1) but with Ψ in the gas and small dust = 0.4.

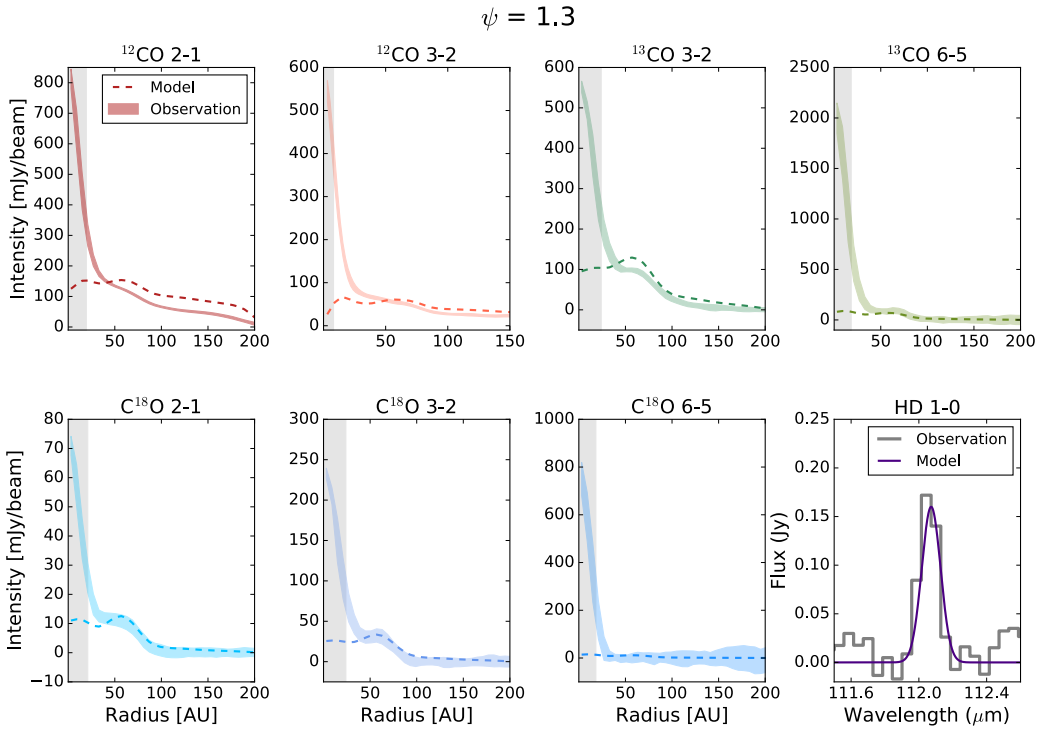

Figure A.5 The integrated intensity profiles of observations and a model based of the initial model (A.1) but with Ψ in the gas and small dust = 1.6.

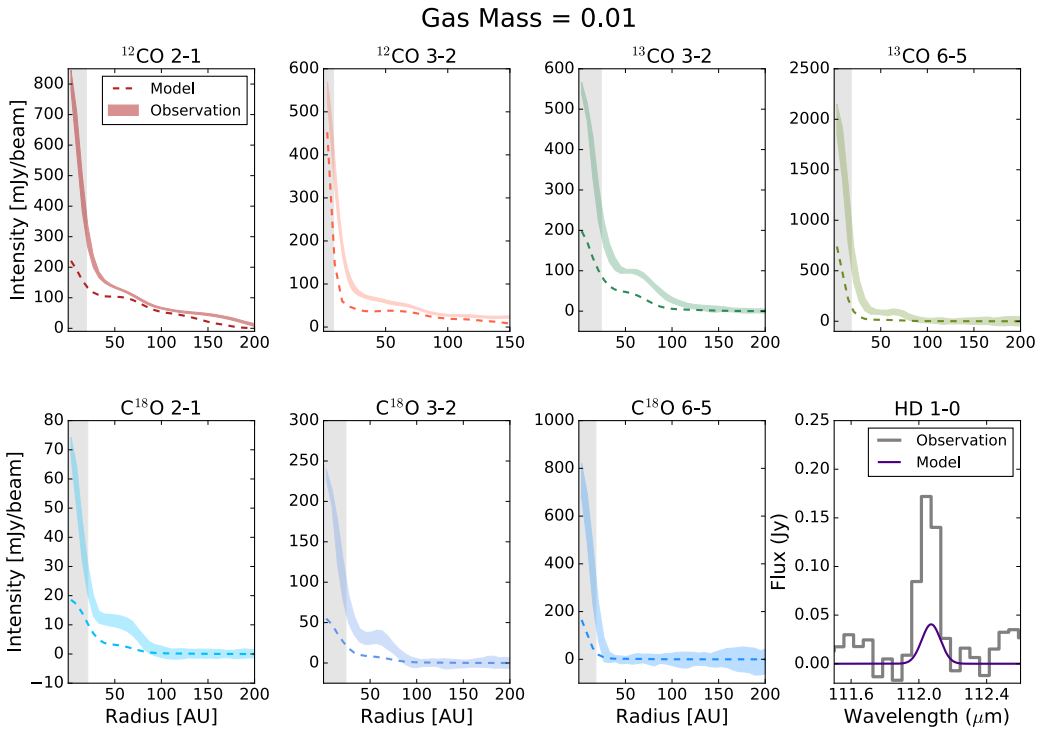

Figure A.6 The integrated intensity profiles of observations and a model based of the initial model (A.1) but with a gas mass equal to 0.01 $M_\odot$

A.1.3 Gas Mass

An increase in the total gas mass increases the intensity from each line along all radii. A higher gas mass results in a higher column density for each molecule, and some of the CO lines (especially ^{12}CO 2-1) are already optically thick in explored mass range. There are also isotopologues whose emission is not fully optically thick in the lower mass models, thus changes in their column have a strong effect on their flux. Increasing the gas mass from 0.01 to 0.02 $M_\odot$ doubles the peak integrated flux in C^{18}O, a 25% increase in ^{13}CO, and ^{12}CO 3-2 and an increase of $\sim$ 20% in ^{12}CO 2-1. Our best-fit model has a disk mass of 0.023 solar masses. We arrived at this value only after the gas and small dust components of our model were given different Ψ values. With a gas mass of 0.05 $M_\odot$ and $\Psi_{\rm gas}$ = 1.1 and $\Psi_{\rm small\ dust}$ = 1.2, the HD flux increases by a factor of two, and emission in CO at large radii also increases by a factor of 2-3 depending on the isotopologue. Due to this, a decrease in total gas mass is justified. Decreasing the mass to 0.023 $M_\odot$ brings the HD flux back down to what *Herschel* observed, and brings the CO emission back down to values that agree with ALMA observations.

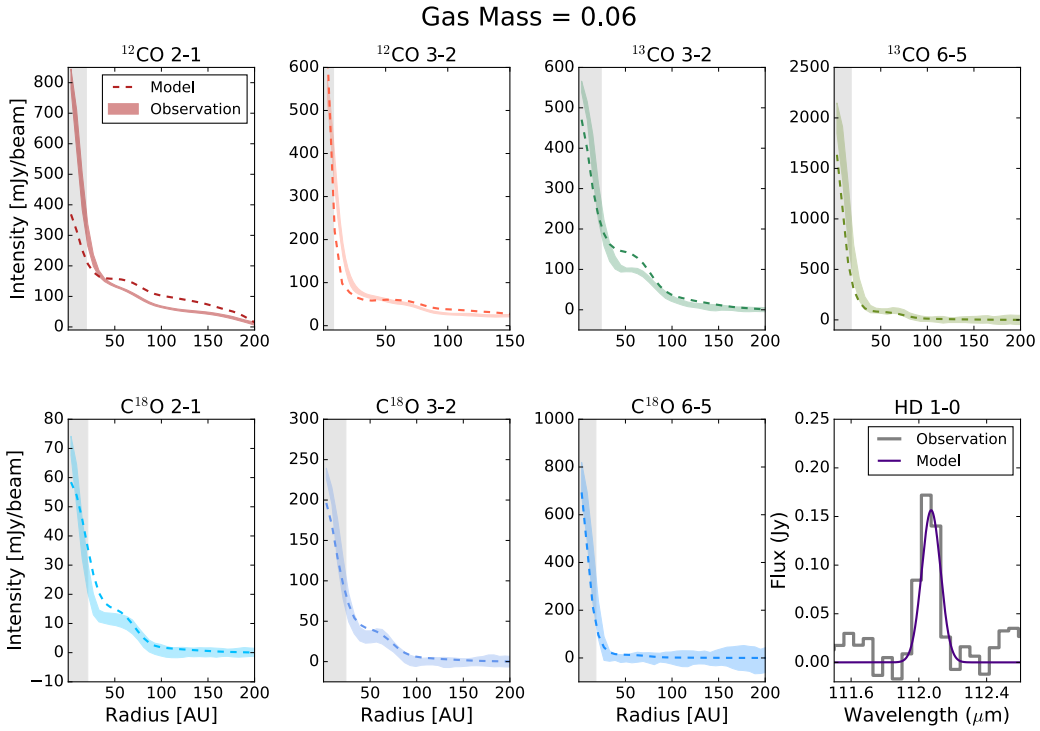

Figure A.7 The integrated intensity profiles of observations and a model based of the initial model (A.1) but with a gas mass equal to 0.06 $M_\odot$

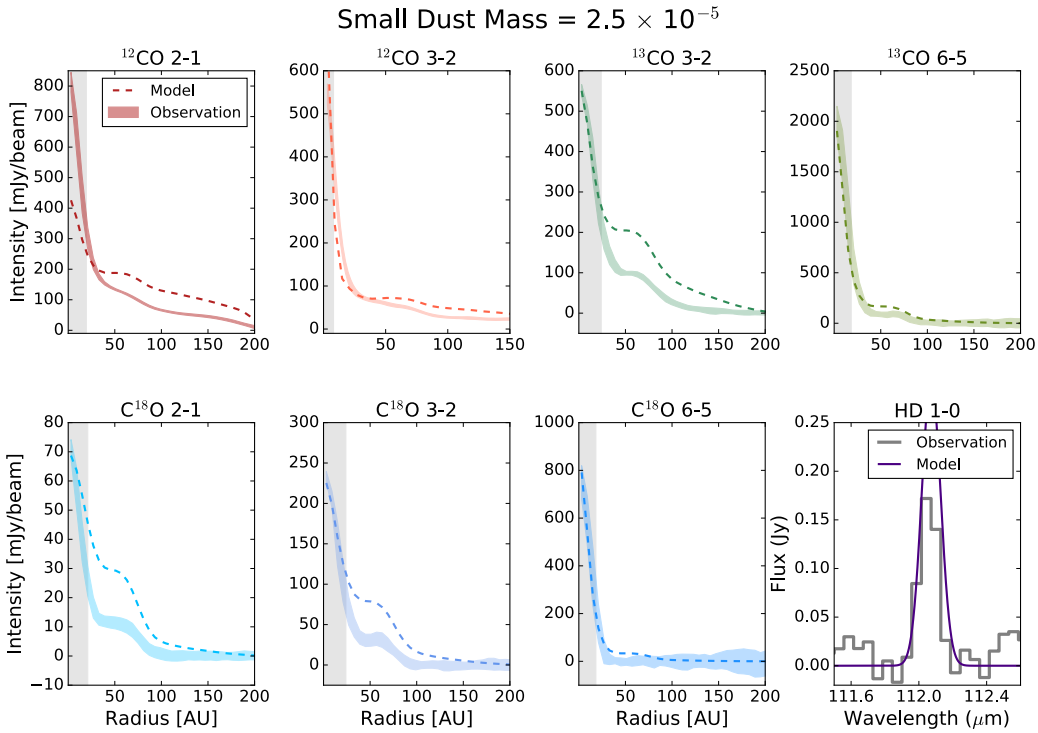

Figure A.8 The integrated intensity profiles of observations and a model based of the initial model (A.1) but with a total small dust mass equal to 2.5 $\times$ 10^{-5} $M_\odot$

A.1.4 Small Dust Component Mass

Given a constant gas mass of 0.05 $M_\odot$ and a starting small dust mass of 1.0 $\times 10^{-4}$ $M_\odot$ or higher, decreasing the small dust mass has a similar effect as increasing gas mass. At 1.0 $\times 10^{-4}$ $M_\odot$ and lower, flux beyond 20 AU increases at a faster rate than within 20 AU, leading to exaggerated features, such as the plateaus in $C^{18}O$ 2-1 and 3-2 becoming peaks at small dust masses less than 2.5 $\times 10^{-5}$ $M_\odot$. The small dust population absorbs and scatters radiation and in some instances leads to a CO line profile that is extincted. Eliminating small dust allows for the gas that exists to emit more freely as a major opacity source is removed. The small dust mass is particularly impactful on the HD emission, because the small dust governs the propagation of UV radiation, with smaller dust masses allowing UV photons from the star to penetrate deeper layers of the disk, directly affecting the gas heating terms. This helps populate the HD J=1 level, increasing the HD J=1-0 line flux. In our final model, we were not strongly motivated to change the small dust mass beyond what had been initially predicted, but it could be a useful lever in future modeling of disks. At present the strongest constraint on the mass of the small dust is the SED and scattered light emission form the surface.

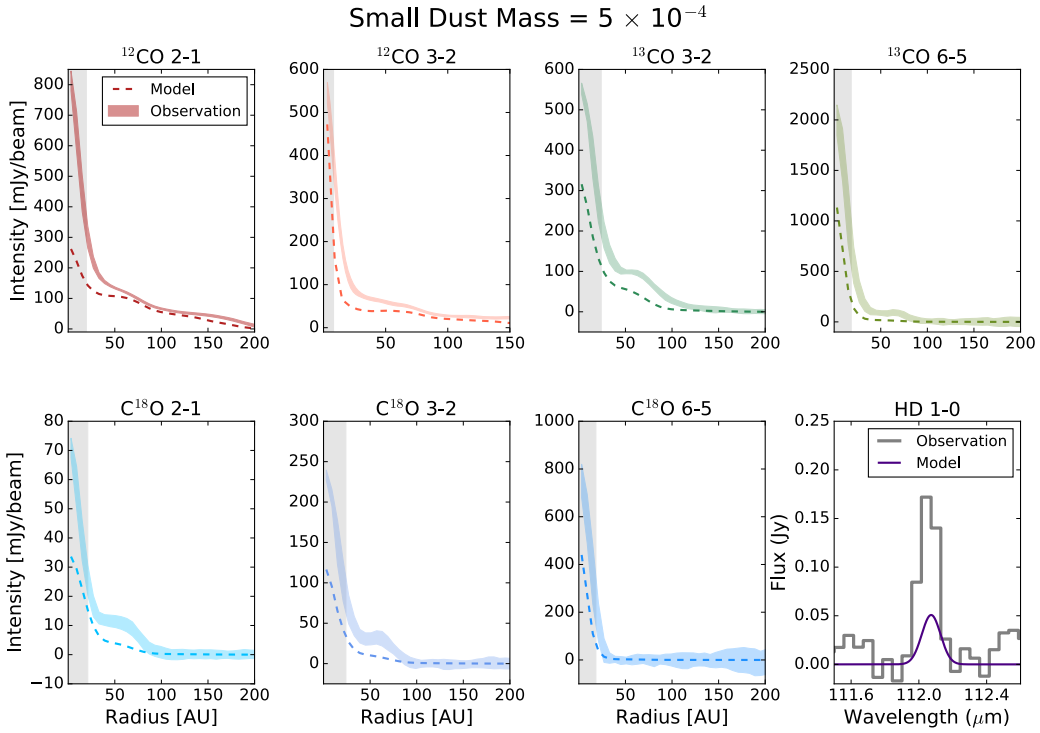

Figure A.9 The integrated intensity profiles of observations and a model based of the initial model (A.1) but with a total small dust mass equal to 5×10^{-4} $M_{\odot}$

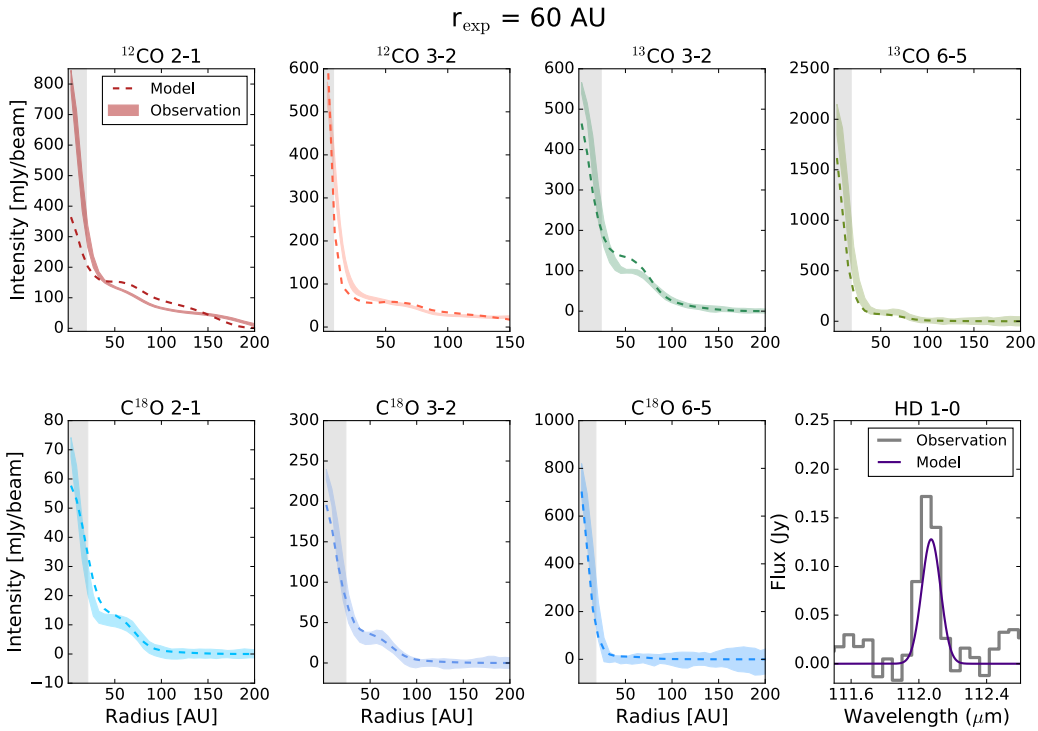

Figure A.10 The integrated intensity profiles of observations and a model based of the initial model (A.1) but with $r_{exp_{out}}$ in the gas and small dust = 60 AU

A.1.5 r_{exp} : Outer Tapering Radius

At this specified radius the abundance of a component exponentially decreases. Altering the r_{exp} effects outer disk emission, as it significantly depletes the corresponding component. It is only significant in ^{12}CO 2-1 and 3-2, as these are the only intensity profiles with emission beyond 100 AU. If the gas and small dust r_{exp} value becomes less than the large dust r_{exp}, the effect is much stronger and acts similar to decreasing γ.

A.1.6 h_c: Characteristic Height

An increase of the height of the disk results in an increase in intensity across all radii and in all molecules, with the ones most strongly affected being the least abundant. A change in scale height increases the column that one observes, which then increases the flux of an optically thin molecule. However, this does not strongly affect optically thick molecules. An increase of two times the scale height only results in a $\sim$ 5 % increase in peak intensity in ^{12}CO 2-1 and a full 20% increase in the least common isotopologue transition considered here, C^{18}O 6-5.

The scale height, scale radius, Ψ, and γ of the large dust population do not have strong effects

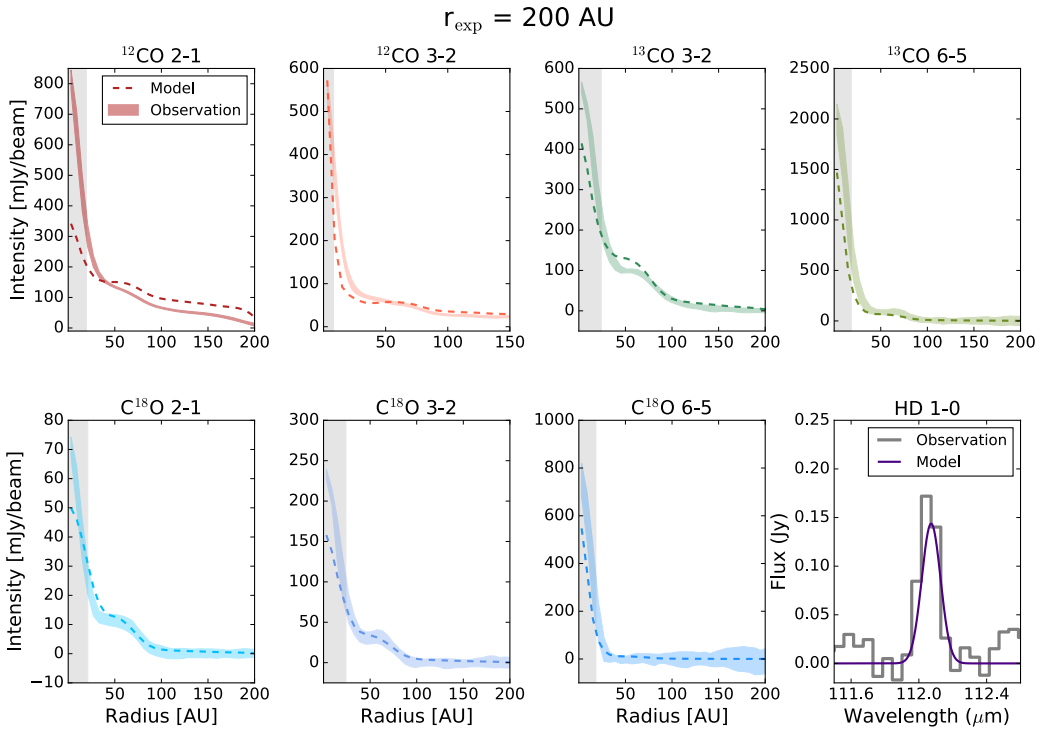

Figure A.11 The integrated intensity profiles of observations and a model based of the initial model (A.1) but with $r_{exp_{out}}$ in the gas and small dust = 200 AU

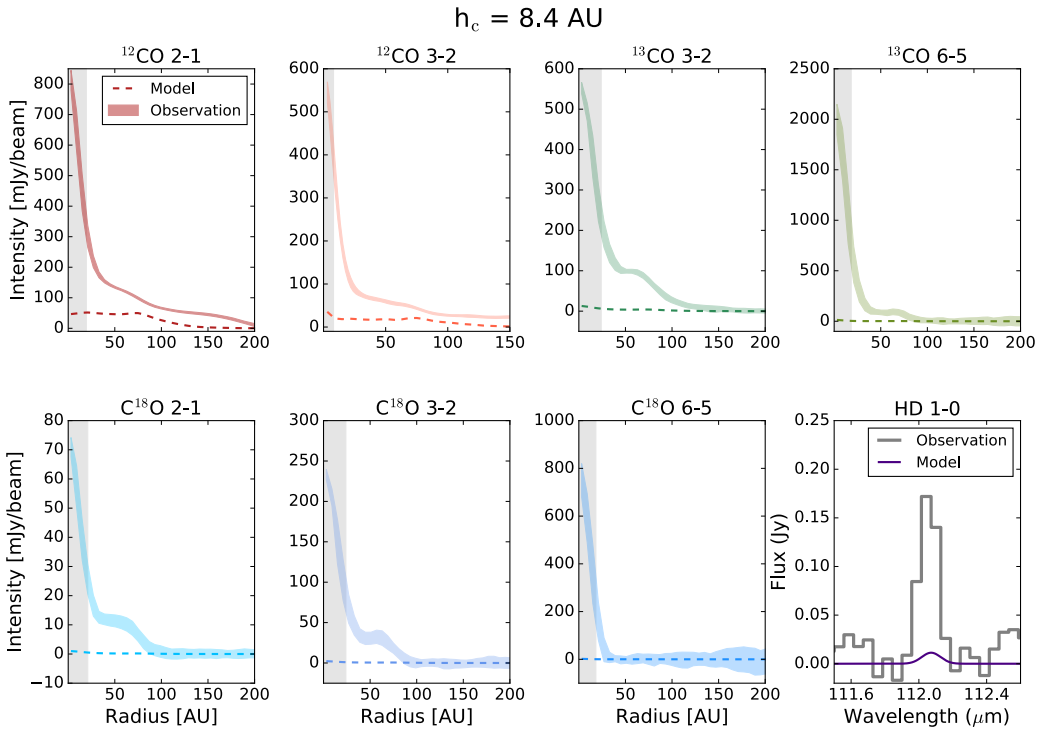

Figure A.12 The integrated intensity profiles of observations and a model based of the initial model (A.1) but with h_c in the gas and small dust = 8.4 AU

on the CO line profiles. The temperature of the star also does not have a strong effect; a change in 1000 K resulted in only a 1% increase across all lines.

The parameters we find having the largest impact on the CO and HD flux were: gas mass, the flaring parameter Ψ, surface density distribution parameter γ, and small dust mass. The gas mass affects all CO lines, and has a stronger influence on the optically thin lines. Ψ and γ both redistribute flux between the inner and outer regions of the disk depending on where the majority of the gas component is located. The small dust mass was not a parameter that needed to be altered from its initial value, but has a strong effect on the HD flux and could be utilized in future studies as long as the SED is taken into account.

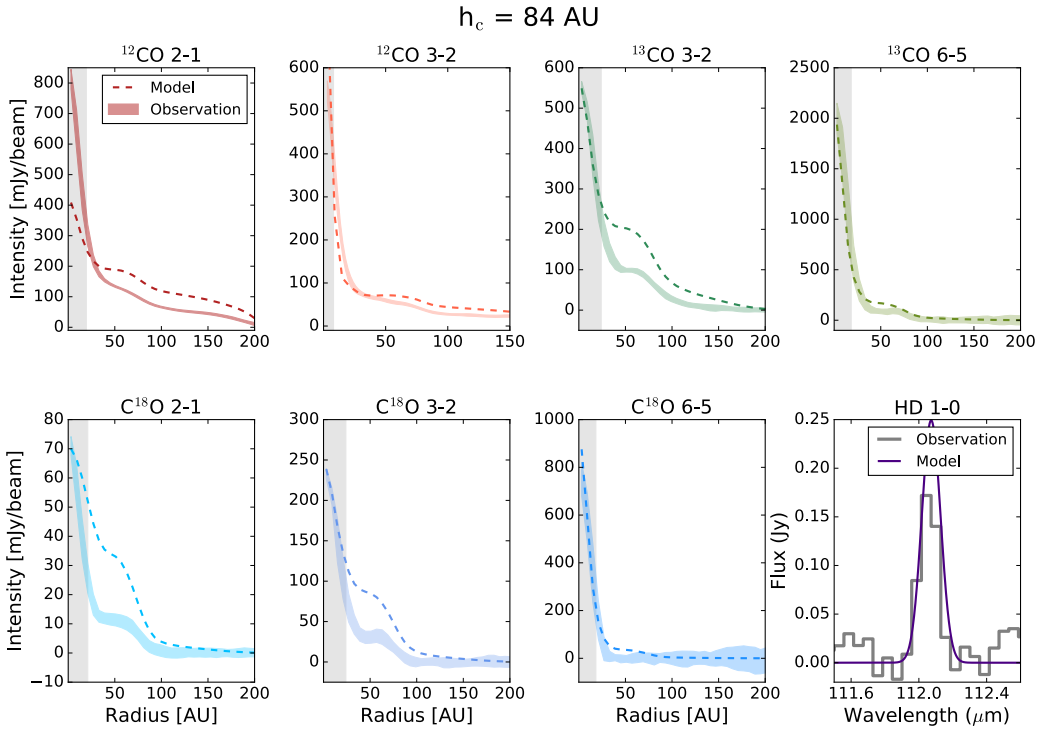

Figure A.13 The integrated intensity profiles of observations and a model based of the initial model (A.1) but with h_c in the gas and small dust = 84 AU

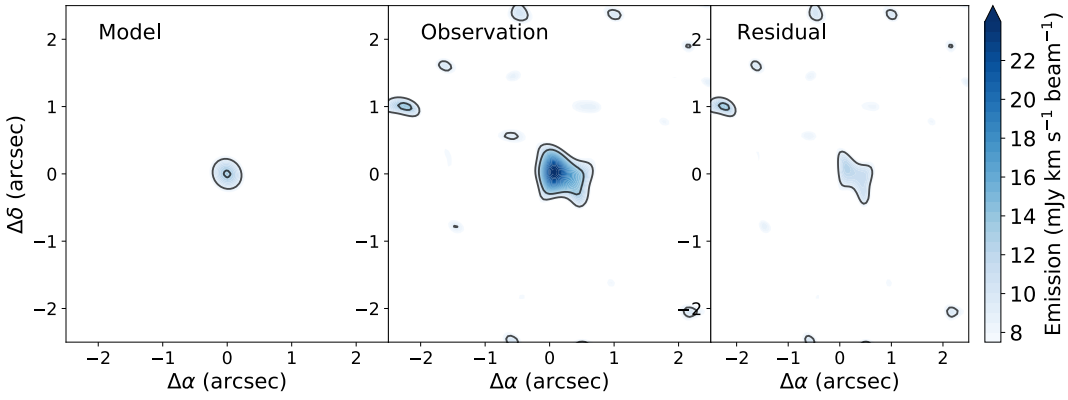

Figure A.14 ALMA observation of ^{13}C^{18}O J=3-2 line emission (middle panel) as compared to our final TW Hya modeled ^{13}C^{18}O J=3-2 flux (left panel), and the residual (right panel). Contours are trace the location of 9 and 13 mJy flux values.

APPENDIX B

HD 163296 Temperature Appendix

B.1 Parameter Exploration Analysis

Our model of the HD 163296 disk based on the density structure from Z21 with an updated CO depletion profile reproduces radial profiles from all lines except ^{12}CO J=2-1 relatively well (see Figure B.1). Thus, this initial model appears to roughly represent the 2D thermal structure, but cannot reproduce the disk layers at which ^{12}CO J=2-1 emission originates, as this line is underpredicted by a factor of about two within the brightest region (within 50 au). However, improvements can be made to all lines except for C^{18}O J=2-1 (and arguably ^{13}CO 1-0) because they are slightly underpredicted in the inner 75 au, while slightly overpredicted in the outer disk. In order to achieve a more complete and accurate thermal profile, it is worth exploring the sensitivity of the radial emission profiles to the disk physical parameters.

Throughout the parameter exploration, we did not alter the CO depletion profile. We find that the CO depletion is only degenerate with disk physical parameters that affect the total gas mass or mass distribution (γ). When the scale height, characteristic radius, or flaring parameter are changed, we find that there is no single CO depletion profile that brings all lines of CO towards what is observed.

We ran a set of models that explored the parameter space of gas mass, small dust mass, flaring parameter (Ψ), surface density power-index (γ), characteristic radius (r_c), critical height (h_c), and radial extent and allowed for the temperature to evolve in a new physical environment. Because HD 163296 has been widely studied, we determined the range exploration based on literature values. There has been a wide array of gas mass estimates, from as low as 8×10^{-3} up to 0.58 $M_\odot$ (Isella et al., 2007; Williams & Best, 2014; Boneberg et al., 2016; Miotello et al., 2016; Williams & McPartland, 2016; Woitke et al., 2019; Booth et al., 2019; Powell et al., 2019; Kama et al., 2020b). Our initial gas mass is 0.14 $M_\odot$, which is on the higher end, thus we created three models that are lower in mass, and one higher in mass: 8×10^{-3}, 1×10^{-2}, 6.7×10^{-2} (predicted gas upper limit based on the HD 1-0 flux (Kama et al., 2020b)), and 0.21 $M_\odot$ (the HD 163296 disk

mass estimate from Booth et al. (2019)). In terms of small dust mass, the SED constrains the range of exploration. We start with a mass of 1×10^{-4} $M_{\odot}$, and explore values above and below this with the extremes being clear under and over predictions of the SED flux beyond 10μm : 1×10^{-6} $M_{\odot}$, 1×10^{-5} $M_{\odot}$, 1×10^{-3} $M_{\odot}$, 1×10^{-2} $M_{\odot}$. Flaring for HD 163296 has also had a wide range of estimates throughout the literature, and different studies assume both flat and flared disks. We explore models that use Ψ values above and below what we have used (1.08). This includes 0.05, 1.0, 1.6, 2.2 (Tilling et al., 2012; de Gregorio-Monsalvo et al., 2013; Woitke et al., 2019; Kama et al., 2020b). The surface density index, γ, has a natural limit in our description of surface density (see Equation 1). We explore values above and below our initial value of 0.8: 0.2, 0.6, 1.2, and 1.8. There is ^{12}CO J=2-1 detected out to 600 au, thus we only explored values above that for r_{out}: 700, 1000, and 1200 au. For r_c, h_c we explore four values, the lowest of which corresponds to the mm-dust distribution, and the largest being double our initially inferred value.

Changes in gas mass, small dust mass and scale height have similar effects on the CO radial profiles, increasing or decreasing the CO intensity with increasing/decreasing gas mass and scale height and decreasing/increasing small dust mass. Changing the scale height will increase or decrease the CO flux along all radii for all transitions (see B.6), while small dust mass and gas mass effect some lines more than others (see Figures B.2 and Figures B.3). For example, changes in the mass of the gas or small dust populations do not have as strong an effect on ^{12}CO J 2-1 as it does on nearly every other line. While mass changes in these two populations appear to have similar effects, any degeneracy between the two can be broken as the small dust population is constrained by the SED. As the flaring parameter, Ψ, increases, emission is enhanced in the outer disk (the divide between 'outer' and 'inner' disk depends on the characteristic radius). As Ψ decreases, there is a significant increase in the inner disk (see Figure B.5). We found for this model that even small changes in Ψ strongly affect the final radial profile across all lines. The surface density power-index, γ, tends to leave the flux in the inner few au unaffected, but with a smaller γ more emission can be found farther out in the disk (see Figure B.4). This is due to the fact that a smaller γ produces a population that is more evenly distributed. The characteristic radius affects both the height and surface density of a given population, with lower r_c values producing a rapid increase in height and a turn over the surface density at a shorter radius (see Figure B.7). The combination of these two effects produces radial profiles that are brighter for smaller critical radii. The outer radius values we explored did not produce significantly different CO radial profiles, due to the fact that the majority of the emission from all lines exists within 400 au, thus an outer radius cut off well beyond this limit does not affect the observed emission (see Figure B.8).

After this exploration of parameter space, and subsequently creating a number of models that altered multiple parameters simultaneously, we determined that the best set of parameters were the ones that were used by Z21. Keeping with these values, the derived thermal structure matches five

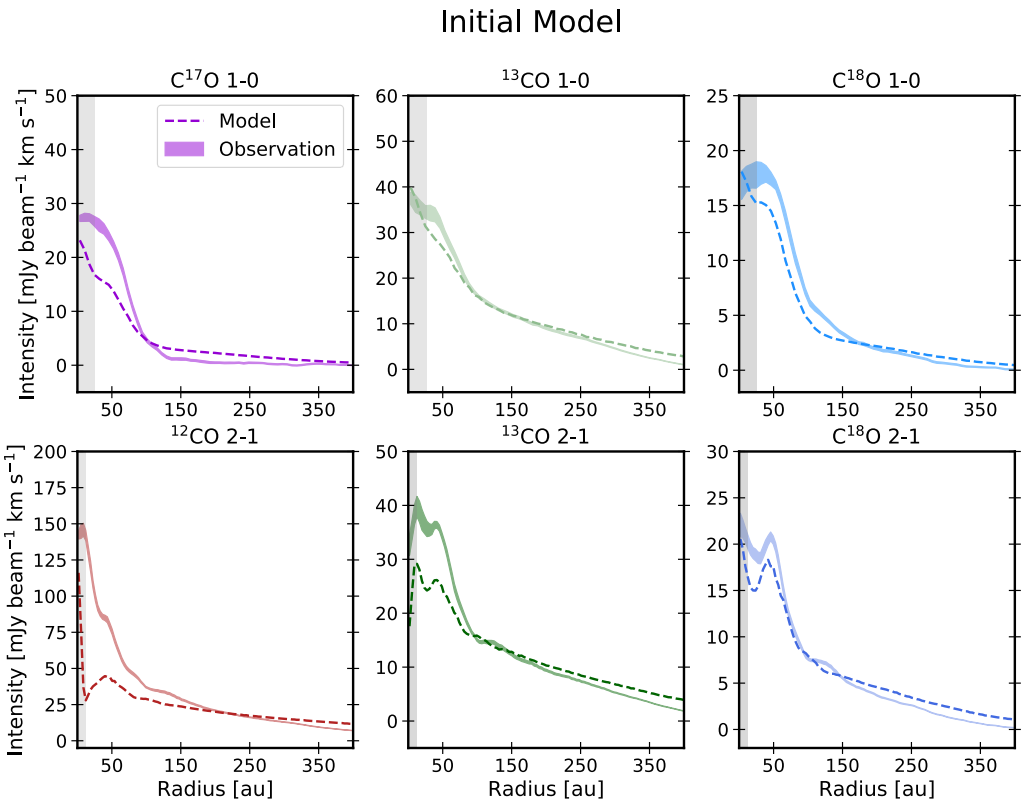

Figure B.1 Radial emission profiles as predicted by the initial HD 163296 model based on Z21 (Z21) compared to the observed profiles (solid line). Parameters are listed in Table 3.3. This model uses the CO depletion calculated in Z21, applied before the temperature calculation, the chemistry runs for 0.01 Myr, and this model lacks the excess heating found necessary to reproduce the ^{12}CO J=2-1 observation

out of six of the radial intensity profiles relatively well and is the best χ^2 fit for the SED (per Z21).

B.2 Gas Temperature Structures in HD 163296 Models from the Literature

There has been one other recent attempt to characterize the 2D thermal structure of the HD 163296 disk specifically, using a thermo-chemical code, matching multiple line observations and the SED. Those results are presented in Woitke et al. (2019). They use the thermo-chemical code ProDiMo (PROtoplanetary DIsk MOdel Woitke et al., 2009; Kamp et al., 2010; Woitke et al., 2016) and derive a disk model that reproduces observed line fluxes from infrared to millimeter wavelengths

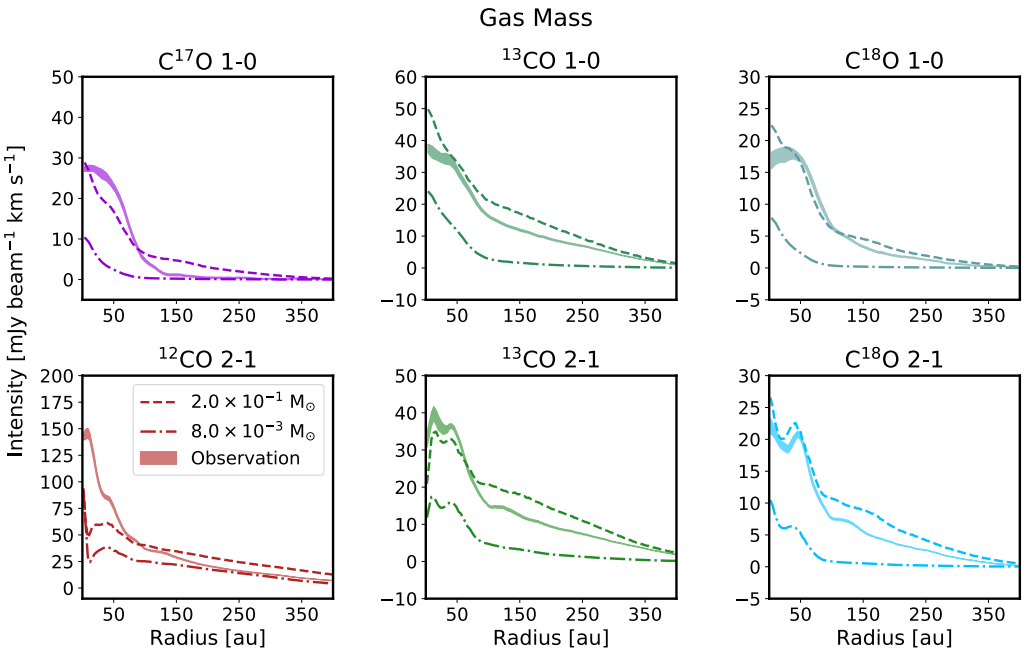

Figure B.2 Modeled radial emission profiles of HD 163296 model based on Z21 compared to the observed profiles (solid line). These models exhibit varying gas mass: 0.2 $M_\odot$ which is a mass prediction for HD 163296 by Booth et al. (2019) and 0.008 $M_\odot$ which is the smallest predicted mass in literature.

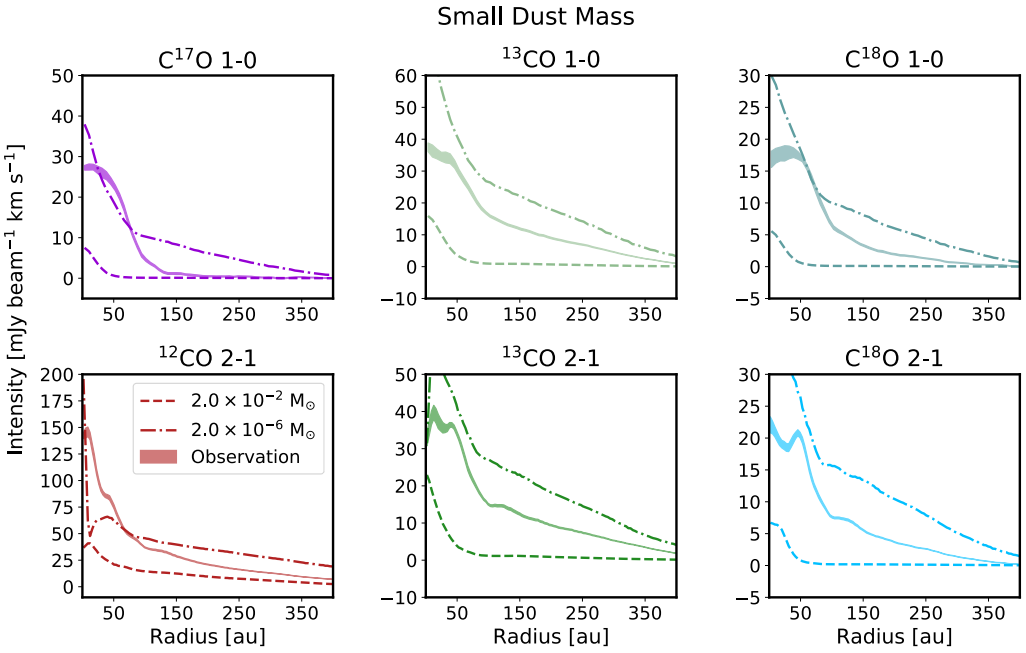

Figure B.3 Modeled radial emission profiles of HD 163296 model based on Z21 compared to the observed profiles (solid line). These models vary in small dust mass: 2×10^{-6} $M_\odot$ and 2×10^{-2} $M_\odot$. The small dust mass is constrained by the SED, and these limits represent dust mass values that are just under and over predicting the SED.

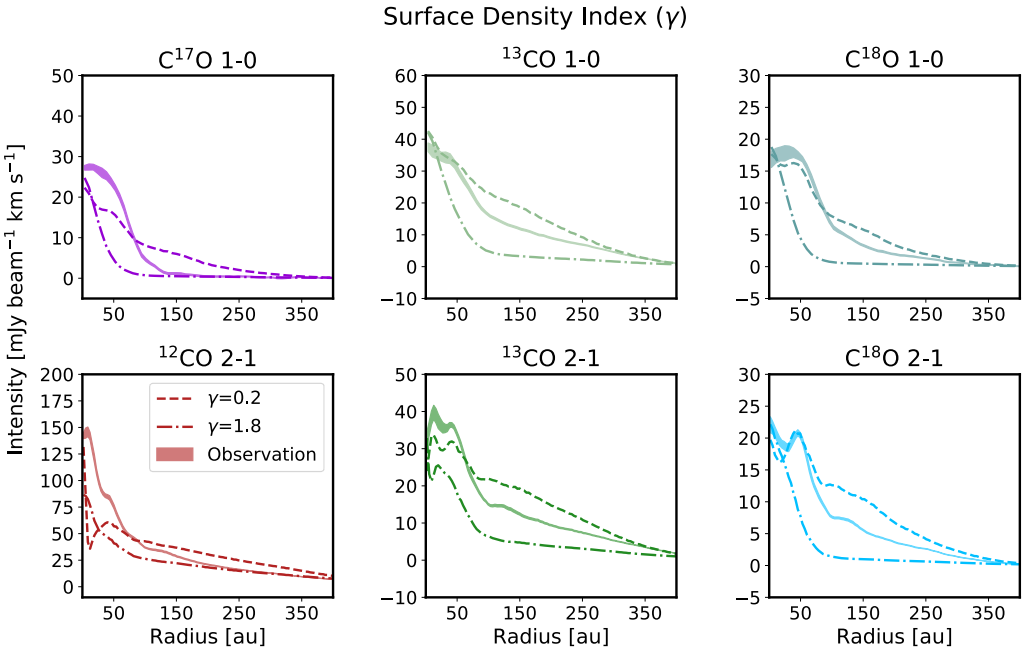

Figure B.4 Modeled radial emission profiles of HD 163296 model based on Z21 compared to the observed profiles (solid line). The models vary in surface density index, γ =0.2 and 1.8. There is a limit for γ of 0 - 2 based on our definition of surface density, thus we explored values at the upper and lower ends of that natural range.

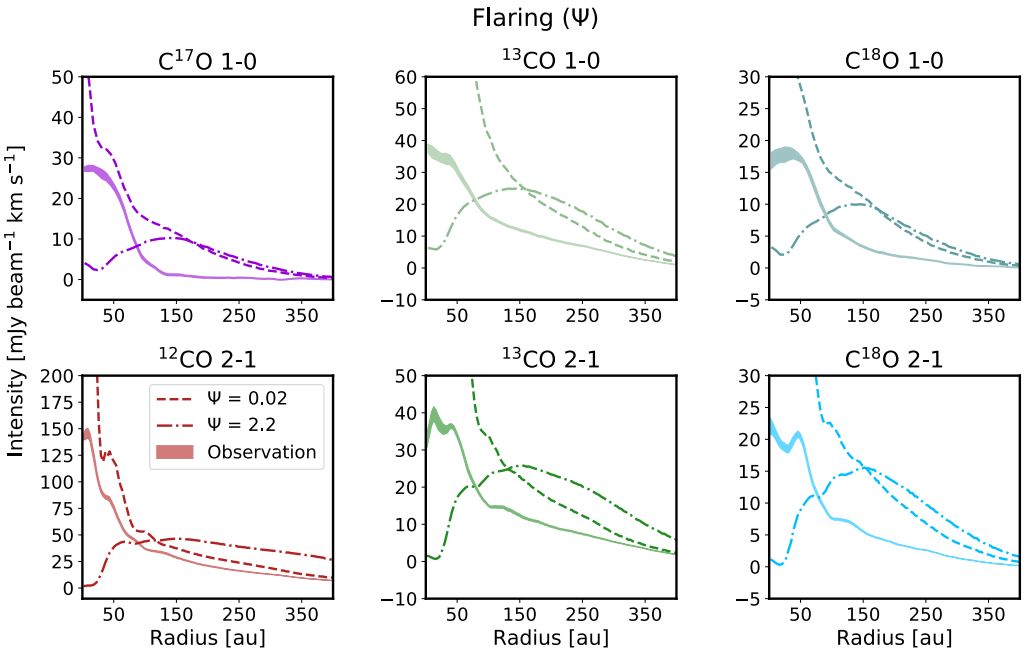

Figure B.5 Modeled radial emission profiles of HD 163296 model based on Z21 compared to the observed profiles (solid line). These models exhibit varying gas mass: 0.2 $M_\odot$ which is a mass prediction for HD 163296 by Booth et al. (2019) and 0.008 $M_\odot$ which is the smallest predicted mass in literature.

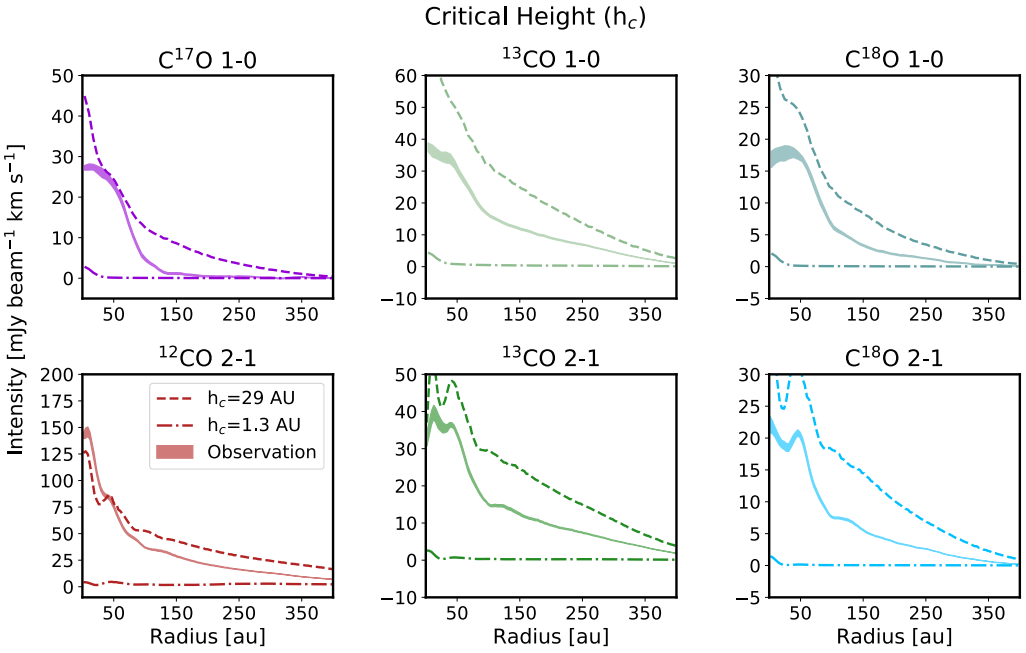

Figure B.6 Modeled radial emission profiles of HD 163296 model based on Z21 compared to the observed profiles (solid line). These models vary in scale height. We explore scale height values as low as what has been used to describe the large grain population, to as high as twice as what we originally predicted.

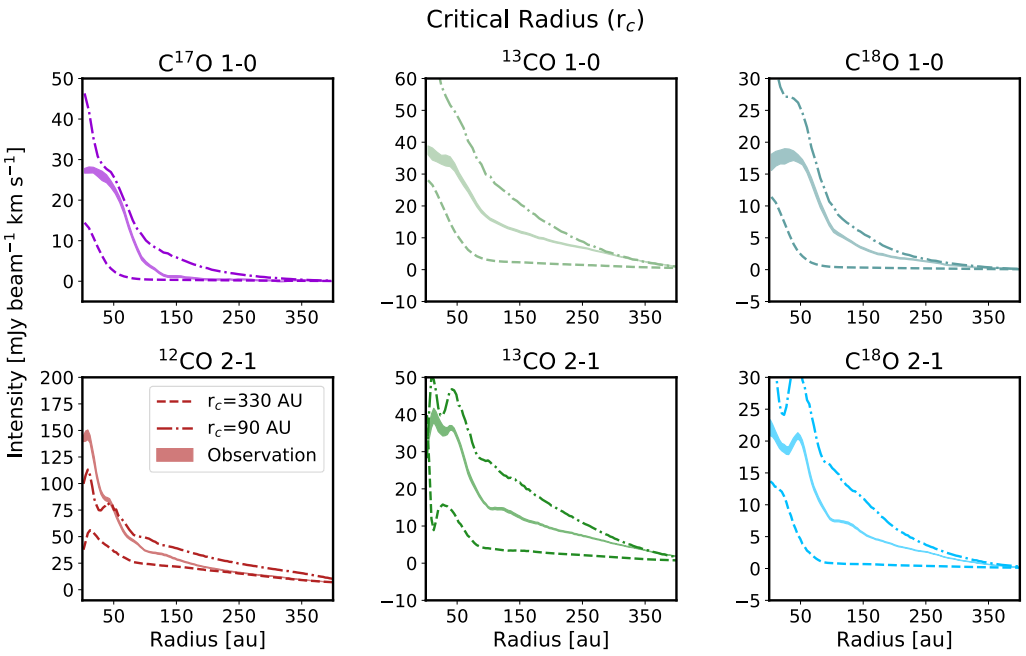

Figure B.7 Modeled radial emission profiles of HD 163296 model based on Z21 compared to the observed profiles (solid line). These models vary in characteristic radius. We explore characteristic radius values as low as what has been used to describe the large grain population, to as high as twice as what we originally predicted.

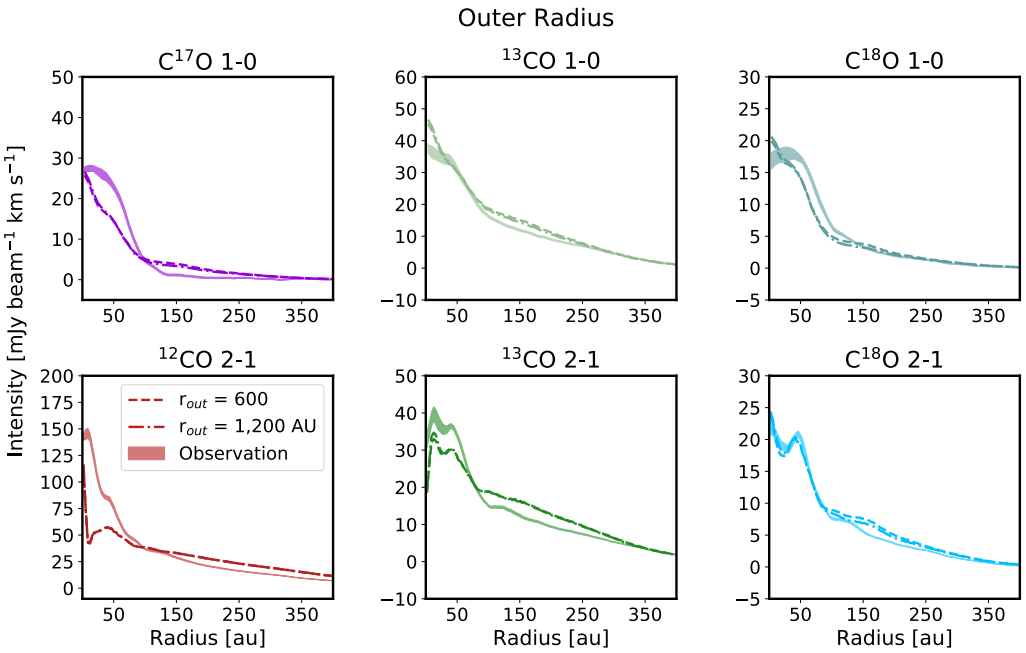

Figure B.8 Modeled radial emission profiles of HD 163296 model based on Z21 compared to the observed profiles (solid line). These models vary in outer radius. We explore radius values as low as 600 au, which is the largest radial extent of the observed ^{12}CO, to twice that size.

within a factor of about two, along with the observed SED. The model outputs from Woitke et al. (2019) are available publicly, and we compare our final thermal structure to their results in Figure B.9. The dust temperatures in both models are very similar, with the disk in our model being slightly more flared. The gas temperatures are very similar within $\sim$ 200 au, while past 300 au the ProDiMo model has a much hotter disk than what this study predicts. That relatively hot temperature most likely would affect the spatially resolved radial profiles, namely ^{12}CO J=2-1 which emits beyond 300 au.

There are a few possible reasons as to why that study did not find it necessary to invoke additional heating in the layers at which ^{12}CO J=2-1 primarily emits. A key difference between the two models is the underlying gas mass; 0.58 $M_\odot$ from Woitke et al. (2019) vs. 0.14 $M_\odot$ in this study (although the ProDiMo model used a pre-Gaia distance of 119 pc, as opposed to the Gaia determined 101 pc). Additionally, the ProDiMo model utilizes an enhanced gas/dust ratio of $>$ 100 throughout the whole disk, and an even higher ratio within the inner few au . In our case, depleting small dust within the inner tens of 10 au in our model did not appear to rectify the difference between predicted and observed ^{12}CO J=2-1. The gas temperature in the inner 4 au of the ProDiMo model is on the order of 500 K or more, which we do not see in our model, and none of our observations constrain gas temperatures at such small scales. ProDiMo specifically models

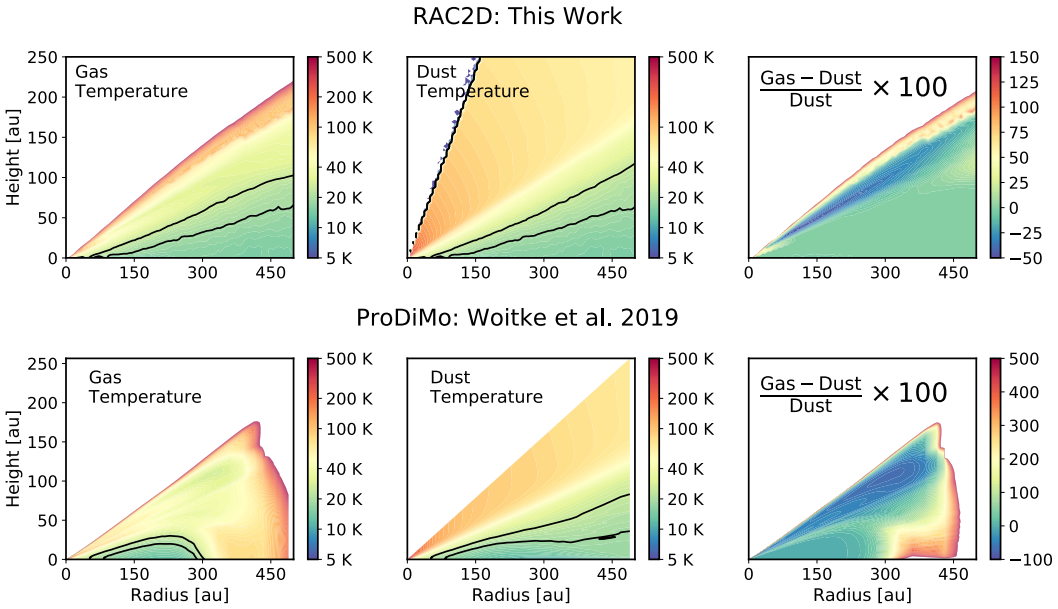

Figure B.9 A comparison between this work's HD 163296 thermal structure that best reproduces the CO radial profiles, and the HD 163296 specific model from Woitke et al. (2019). The two contours in black follow 19K and 25K.

the inner disk separately from the outer disk, and the temperature within this region is significantly warmer than the outer disk region.

Table B.1. CO upper level transitions

Transition	**Model Flux**	**Observed Flux**	**Model in**
	Integrated Intensity [1×10^{-17} W m^{-2}]		**Observed Range?**
5-4	0.504	1.04 ± 0.4	2σ
6-5	0.677	0.74 ± 0.29	1σ
7-6	0.807	0.9 ± 0.3	1σ
8-7	0.847	1.24 ± 0.55	1σ
9-8	0.766	0.91 ± 0.4	1σ
10-9	0.628	1.17 ± 0.35	2σ
11-10	0.566	1.13 ± 0.35	2σ
12-11	0.586	1.17 ± 0.35	2σ
13-12	0.606	1.52 ± 0.4	3σ
14-13	0.626	<1.6	True
15-14	0.648	1.03 ± 0.5	1σ
16-15	0.668	<1.3	True
17-16	0.680	0.75 ± 0.25	1σ
18-17	0.682	<0.9	True
19-18	0.671	<0.9	True
20-19	0.65	<0.9	True
21-20	0.621	<0.9	True
22-21	0.587	<0.9	True
23-22	0.549	<0.9	True

Note. — Observed flux values are from Fedele et al. (2016) and references therein. Quoted errors are the 1σ noise measured in the continuum nearby each line. The right-most column shows whether the modeled flux agrees within 1, 2, or 3σ of the observation, or 'True' if the modeled flux is below an upper limit.

APPENDIX C

UV-Chemistry Supplementary Information

UV-Chemistry Appendix

TW Hya

We additionally produced a thermo-chemical model representing the disk around T Tauri star TW Hya. TW Hya is approximately 10 Myrs old(Thi et al., 2010) and hosts the closest Class II disk at 59.9 pc(Gaia Collaboration et al., 2018). TW Hya has been widely observed in multiple gas and dust tracers with high spatial resolution ($\sim$10 au)(Andrews et al., 2012; Huang et al., 2018). It also exhibits bright CH_3CN coming from $\sim$33 K gas(Loomis et al., 2018). Our modeling efforts of TW Hya follow that of Calahan et al. 2021a(Calahan et al., 2021c) which sets up a thermo-chemical model of the disk by reproducing the spectral-energy distribution (SED), the full line intensity and morphology of seven CO isotopologue transitions, and an HD J=1-0 observation from the *Hershel* PACS instrument(Bergin et al., 2013). To reproduce all CO radial profiles as well as the HD flux, the small dust in the upper layers of the atmosphere of the TW Hya disk were effectively depleted slightly(Calahan et al., 2021c) due to having a slightly lower flaring angle than the gas population. This was enough small dust depletion to reproduce the available CH_3CN lines from Loomis et al. 2018a given a C/O ratio equal to 1.0 (see Figure C.1). This disk is an additional piece of evidence supporting our evolved chemistry proposal.

Implications on Other Molecules

This introduction of a late-stage photo-chemical equilibrium was motivated by observations of CH_3CN, HC_3N, and HCN. However, the late-stage chemistry would have an effect on other molecules as well. We predict in addition to these organic molecules, molecules such as C_XH, C_XH_2, and HC_XN will be abundant in the gas, enhanced by the cycle of carbon chemistry that reproduces observed CH_3CN and HC_3N. The main carbon carrier, CO, is largely unaffected by the increase in photo-chemistry. CO is largely in the gas phase in previous models that do not include

this 'late-stage' chemistry and in the region in which CH_3CN was added into the gas, CO was already primarily in the gas phase. We find a slight depletion of CO in the upper atmosphere of the disk due to the CO photodissociation layer being pushed down, and there is a slight enhancement of CO in the midplane due to the UV-enhancement. However this accounts for less than 1% of the total abundance of CO thus did not have a strong impact on the modeled radial profiles. Another key molecule is H_2O. In our models, we do not initialize our model with H_2O, thus there is very little water to be affected by this 'late-stage' chemistry. Observational results of Du et al. 2017(Du et al., 2017) support this as they found a low overall abundance in H_2O in disks with a survey of 13 protoplanetary disks. CH_3CN nor HC_3N would be seen to be at a high abundance if gas-phase H_2O was in high abundance in the disk as it would disrupt the carbon-rich chemistry.

SED Degeneracy

The depletion of small grains will affect the observed spectral energy distribution (SED) from each disk. TW Hya's dust population was not altered from that of Calahan et al. 2021a(Calahan et al., 2021c) and continues to match its observed SED. A depletion of a factor of 10 in the small dust population around HD 163296 would cause a dimming in the mid-infrared part of the SED. However, the small dust abundance, the distribution of dust grain size, and the assumed dust opacity sources are degenerate in the ways they may affect the disk SED. We modeled protoplanetary disk SEDs using the code TORUS(Harries et al., 2004, 2019). TORUS is a Monte Carlo radiative transfer code utilizing radiative equilibrium(Lucy, 1999) and silicate grains(Draine & Lee, 1984). In Figure C.7, we show a series of SEDs produced from models motivated by our thermo-chemical model of HD 163296 including the stellar parameters and dust distribution in Table 1 from Calahan et al. 2021b(Calahan et al., 2021b). We find that by varying the minimum dust grain radius or the power law index, we can account for a factor of 10 in UV attenuation. The total population mass, grain size, and how the grain sizes are distributed are strongly degenerate and can result in uncertainties of the dust mass by a factor of at least 10. Thus our depletion of small dust continues to reproduce all previous observables including the SED.

MRI Instability

With the increase in UV flux deeper into the disk, more ions are created. Ions can be coupled with the magnetic fields that thread through the disk and interact with the bulk gas creating turbulence. This mechanism is called the magneto-rotational instability or MRI(Balbus & Hawley, 1991). Magneto-hydrodynamical processes are assumed to be present throughout protoplanetary disks due to young star's active magnetic field, and are thought to be one of the main drivers of angular momentum transport (Chandrasekhar, 1960). An MRI-active zone may drive the bulk of

the mass transportation in the disk and activate accretion onto the star, two vital processes that determine the future of a young solar system. It is thought that planet formation may be aided within 'dead-zones' where MRI is non-active(Gressel et al., 2012). The magnetic Reynolds number (Re) and ambipolar diffusion term (Am) are two quantities that help quantify the presence of an MRI-active zone. The Reynolds number quantifies the level of coupling between ionized gas and magnetic fields and is defined as

$$Re \equiv \frac{c_s h}{D} \approx 1 \left(\frac{\chi_e}{10^{-13}}\right) \left(\frac{T}{100\ \mathrm{K}}\right)^{1/2} \left(\frac{a}{\mathrm{AU}}\right)^{3/2}, \tag{C.1}$$

where c_s is the sound speed, h is the scale height of the disk, D is the magnetic diffusivity parameter, χ_e is the electron abundance, T temperature and a radial location in the disk (Perez-Becker & Chiang, 2011). The ambipolar diffusion term describes the coupling of ionized molecules and their interaction with neutral gas particles:

$$Am \equiv \frac{\chi_i n_{\mathrm{H_2}} \beta_{\mathrm{in}}}{\Omega} \approx 1 \left(\frac{\chi_i}{10^{-8}}\right) \left(\frac{n_{\mathrm{H_2}}}{10^{10}\mathrm{cm}^{-3}}\right) \left(\frac{a}{\mathrm{AU}}\right)^{3/2}, \tag{C.2}$$

where χ_i is the ion abundance, $n_{\mathrm{H_2}}$ is the number density of H_2 atoms, Ω is the dynamical time, β_{in} is the collisional rate coefficient for singly charged species to share momentum with neutral species, and a is the radial location in the disk (Draine et al., 1983; Perez-Becker & Chiang, 2011). For MRI to act as a turbulent driver of neutral gas, both Re and Am must be sufficiently high. Simulations show that values between 0.1-100 for Am can trigger significant coupling between ions and neutrals (Hawley & Stone, 1998; Bai & Stone, 2011). Models by Flock et al. 2012(Flock et al., 2012) suggest $Re \approx$ 3,300-5,000 is required to sustain sufficient turbulence with a critical Re = 3,000. In our work, we assume a combined $Am >$100 and $Re >$ 3,000 to signify an MRI-active zone.

We calculate the regions in which the MRI is active in the HD 163296 disk in our models with an early-stage physical environment and a late-stage environment (signified by a depletion in the small dust population mass) in Figure C.4. Our solution allows for an increase of UV flux in the atmosphere by a factor of 3-5. More of the disk becomes ion-rich due to the CO and H_2 self-shielding layers being located deeper into the disk. The increase in the ion and electron abundance (χ_i, χ_e) are the key factors that enhance the Re and Am values and thus produce additional MRI activity (see Figure C.4). As a result, thirteen times more mass within the disk becomes MRI-active including within the midplane. In the base model representing early stages of disk chemistry, the MRI activity at the midplane extends to 4 au. By depleting the small dust population by an order of magnitude, the MRI activity at the midplane then extends out to $\sim$10 au. This increase in MRI activity can contribute to the reason behind why older disk systems, such as TW Hya, are actively accreting. Meridional flows have been identified in the HD 163296 disk located at two

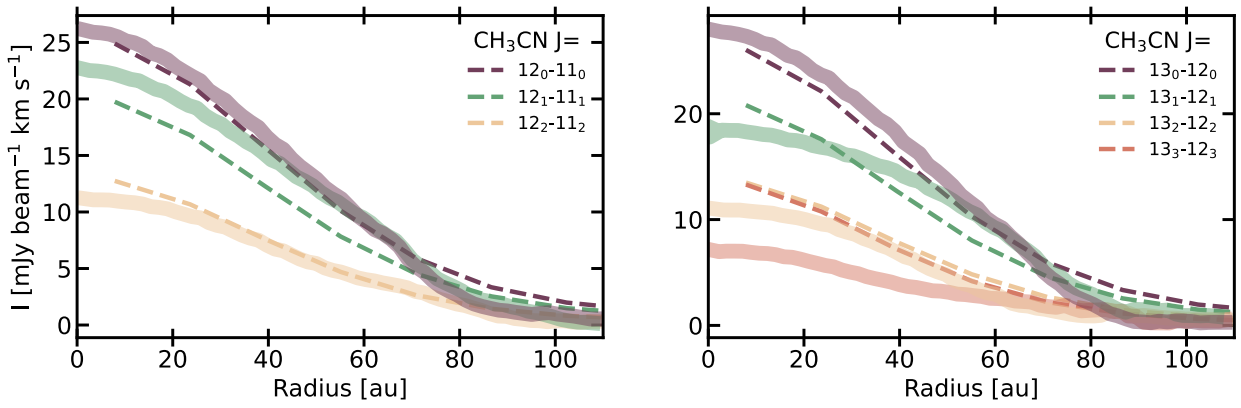

Figure C.1 A comparison of observed CH_3CN(Loomis et al., 2018) towards TW Hya and a thermo-chemical model. The model is run for 1 Myr with a gas-to-dust ratio equal to 250 and a C-to-O ratio equal to 1.0. Observed emission is shown as the solid lines while modeled results are the dashed lines. The left and right panels show different J_K transitions.

of the largest dust gaps (approx. 45 and 86 AU)(Teague et al., 2019b) and these vertical flows are coincident with the lower vertical limit of the MRI-active zone. The MRI activation could have an effect on the height or continue to drive meridional flows. Turbulence measurements of the HD 163296 disk have been derived in Flaherty et al. 2015 and 2017(Flaherty et al., 2015, 2017) using molecular tracers, and they find turbulent velocities to be 5% or less of the sound speed between 30-300 au and at all measured heights. It is not yet clear whether our MRI prediction is in tension with the observational evidence of low turbulence in HD 163296, more work needs to be done on the modeling of how MRI-active regions drive turbulence and more observational constraints are needed to constrain the inner 40 au where we find the strongest MRI-activity.

Supplementary Figures

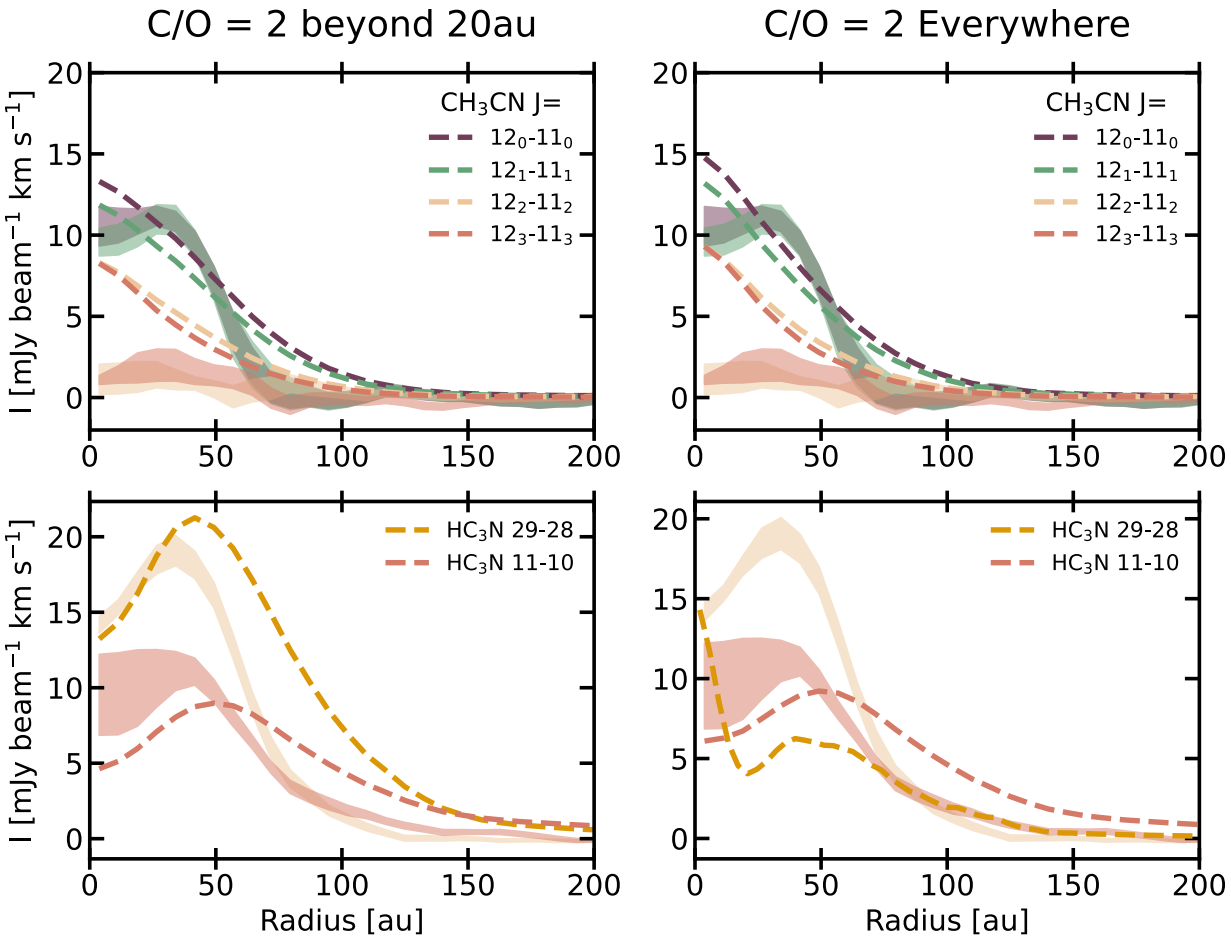

Figure C.2 A comparison of two HD 163296 disk models with varying C-to-O ratios. The final model has a C-to-O = 0.47 within 20 au and C-to-O = 2 beyond 20 au (left). The comparison model has a C-to-O ratio equal 2 throughout the entire disk. Dashed lines are modeled radial intensity profiles while the thick line in the background are observations, with the thickness corresponding to the uncertainty of the flux. In our final model, the C-to-O ratio is equal to what is found in the ISM, 0.47.

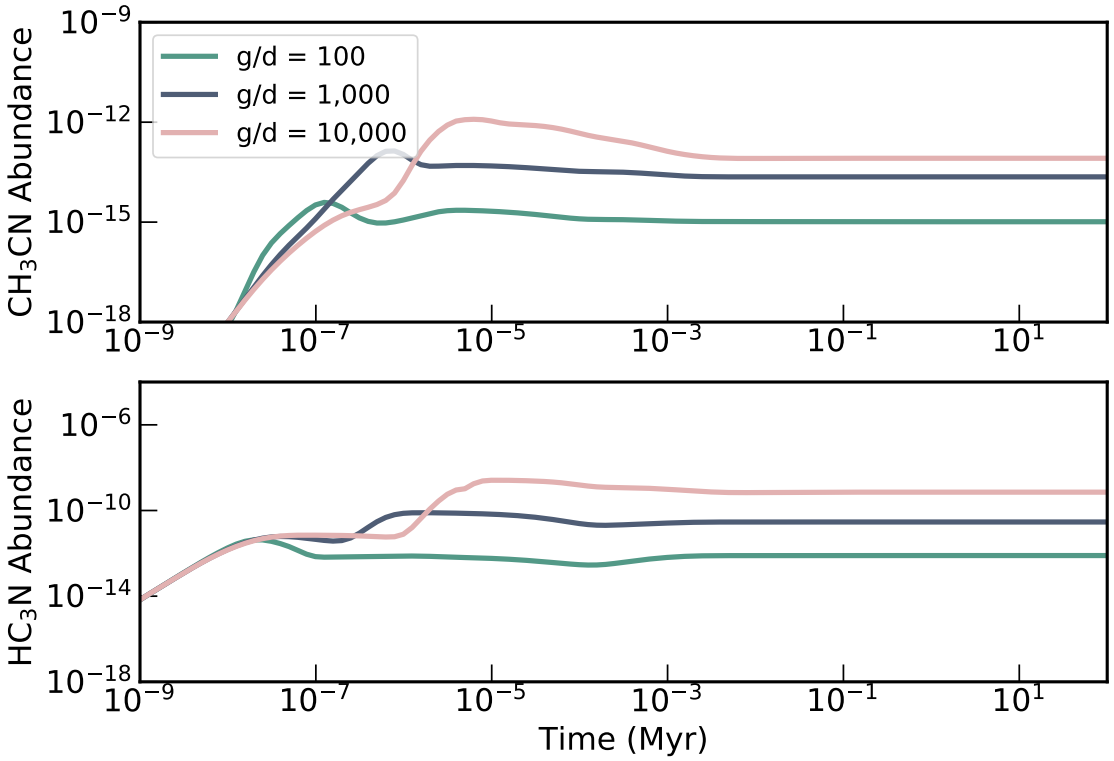

Figure C.3 The evolution of CH_3CN and HC_3N abundances relative to H_2 given different gas to dust ratios. This considers an environment with a 35 K gas and $\mathbf{5 \times 10^{11}}$ mol/cm^3 gas density following our chemical network. The top panel shows the temporal evolution of CH_3CN abundance while the bottom shows the evolution of HC_3N

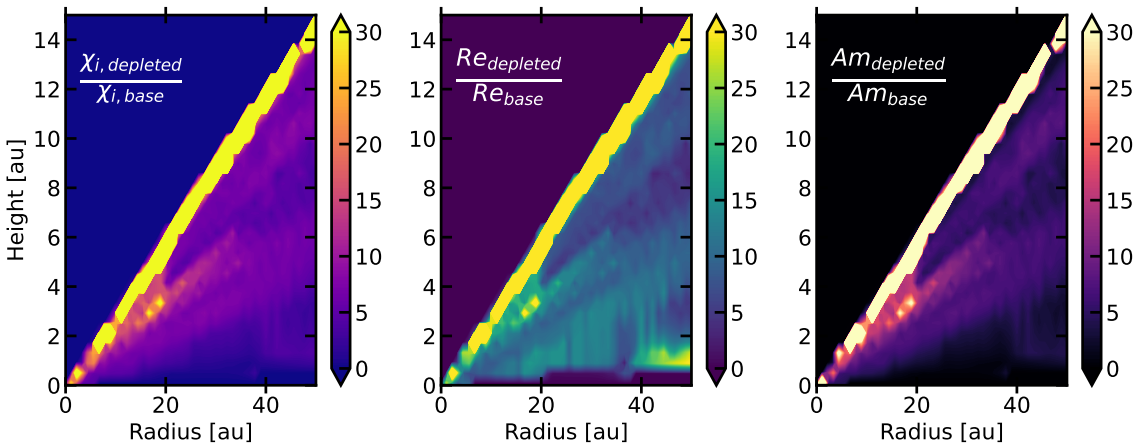

Figure C.4 A comparison of the terms that effect the MRI strength in two distict models. The final ion abundance (χ_i left) calculated Reynolds number (Re, middle) and ambipolar diffusion term (Am, right) are shown in a model depleted of small dust (gas-to-dust = 5,000) versus a baseline model (gas-to-dust = 500). The depleted model corresponds to the model that reproduces observations of CH_3CN, HCN, and HC_3N, see Figure 2 of main text.

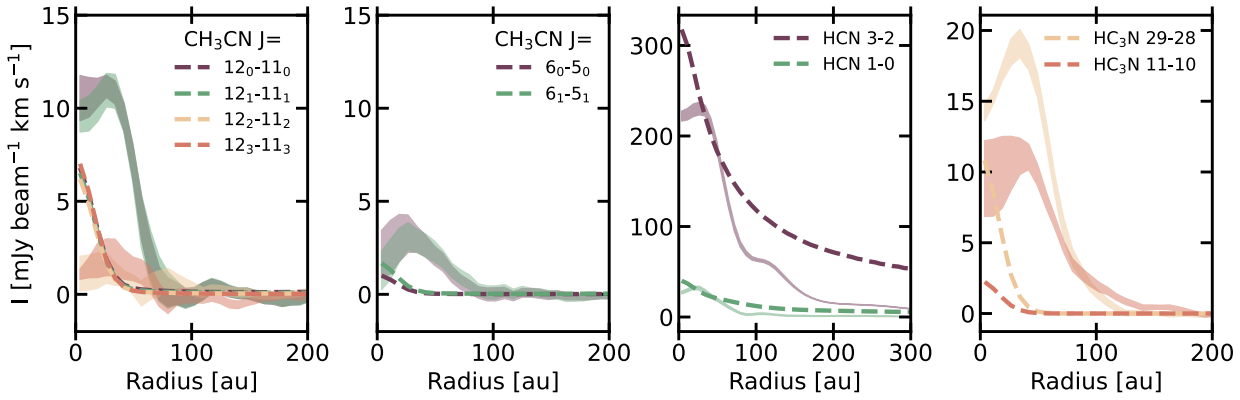

Figure C.5 An HD 163296 model with an elevated C-to-O ratio and normal gas-to-dust ratio in the atmosphere. The model is represented by dashed lines while observations are the thick low opacity lines, where the thickness corresponds to the uncertainty in the flux. The model predicts that each K-line for CH_3CN J=12-11 have nearly identical morphology and intensities. HC_3N is predicted to have a centrally peaked radial intensity profile while observations show a plateau or central dip. By simply decreasing the total mass thus total surface density of the small dust by a factor of 10, the model is much more consistent with observations across all three molecules and their multiple transitions.

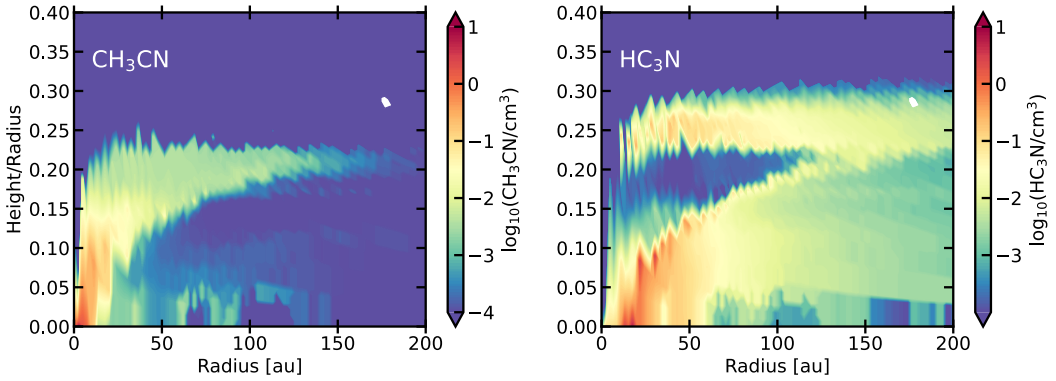

Figure C.6 The radial and vertical number density distributions of CH_3CN and HC_3N in a model with a high C-to-O ratio and normal gas-to-dust ratio. C-to-O is equal to 2 throughout the whole disk, and the atmospheric gas-to-dust ratio is equal to 500 (corresponding to the model results in Figure C.5). This is contrasted with Figure 3, where there is more organic emission deeper in the disk.

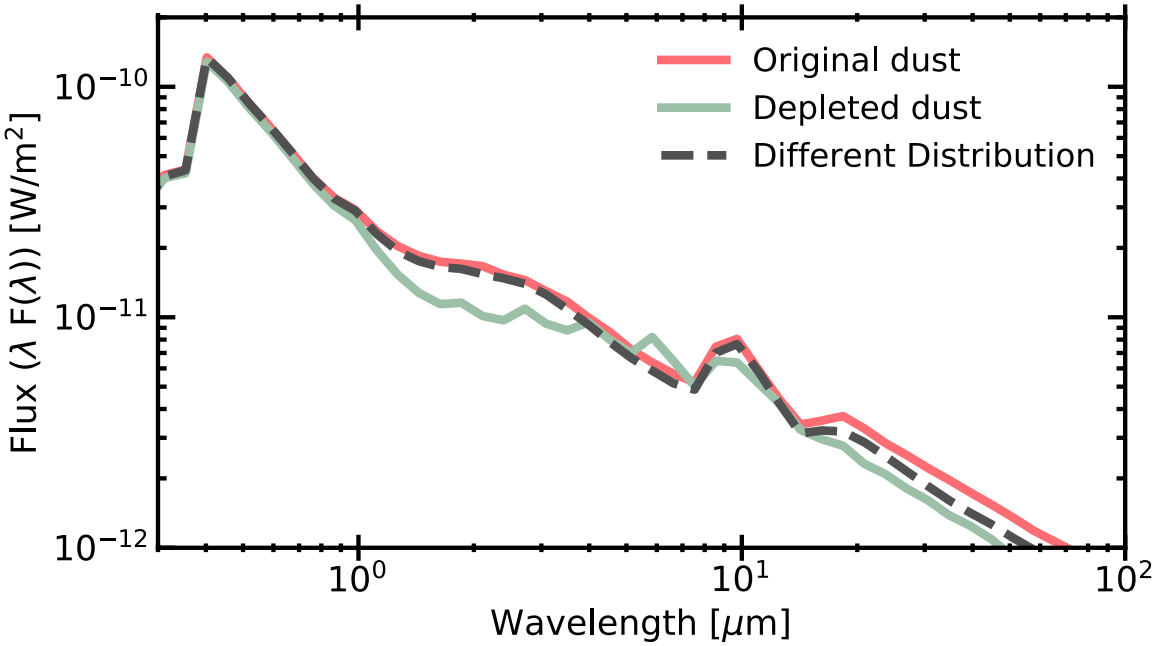

Figure C.7 Three simulated SEDs for different protoplanetary disk dust populations. The 'depleted dust' model has 10 times less mass in the small dust population than the 'Original dust' model. By altering the UV attenuation via increasing the minimum dust radius from 0.005 μm to 0.1 μm (dashed grey line) we reproduce the SED features and intensity as seen in the 'original' model.

BIBLIOGRAPHY

Ábrahám, P., Kóspál, Á., Kun, M., et al. 2018, , 853, 28, doi: 10.3847/1538-4357/aaa242

Aikawa, Y., van Zadelhoff, G. J., van Dishoeck, E. F., & Herbst, E. 2002, , 386, 622, doi: 10.1051/0004-6361:20020037

Alarcón, F., Teague, R., Zhang, K., Bergin, E. A., & Barraza-Alfaro, M. 2020, , 905, 68, doi: 10.3847/1538-4357/abc1d6

Alarcón, F., Bosman, A., Bergin, E., et al. 2021, arXiv e-prints, arXiv:2109.06263. https://arxiv.org/abs/2109.06263

Allen, M., & Robinson, G. W. 1977, , 212, 396, doi: 10.1086/155059

Altwegg, K., Balsiger, H., Combi, M., et al. 2020, , 498, 5855, doi: 10.1093/mnras/staa2701

Anderson, D. E., Blake, G. A., Cleeves, L. I., et al. 2021, , 909, 55, doi: 10.3847/1538-4357/abd9c1

Andrews, S. M. 2020, arXiv e-prints, arXiv:2001.05007. https://arxiv.org/abs/2001.05007

Andrews, S. M., & Birnstiel, T. 2018, in Handbook of Exoplanets, ed. H. J. Deeg & J. A. Belmonte, 136, doi: 10.1007/978-3-319-55333-7_136

Andrews, S. M., Czekala, I., Wilner, D. J., et al. 2010, , 710, 462, doi: 10.1088/0004-637X/710/1/462

Andrews, S. M., Wilner, D. J., Hughes, A. M., et al. 2012, , 744, 162, doi: 10.1088/0004-637X/744/2/162

Andrews, S. M., Huang, J., Pérez, L. M., et al. 2018, , 869, L41, doi: 10.3847/2041-8213/aaf741

Ansdell, M., Williams, J. P., van der Marel, N., et al. 2016, , 828, 46, doi: 10.3847/0004-637X/828/1/46

Ansdell, M., Williams, J. P., Trapman, L., et al. 2018, , 859, 21, doi: 10.3847/1538-4357/aab890

Armitage, P. J., Livio, M., & Pringle, J. E. 2001, , 324, 705, doi: 10.1046/j.1365-8711.2001.04356.x

Aspin, C. 2011, , 141, 196, doi: 10.1088/0004-6256/141/6/196

Asplund, M., Amarsi, A. M., & Grevesse, N. 2021, , 653, A141, doi: 10.1051/0004-6361/202140445

Audard, M., Ábrahám, P., Dunham, M. M., et al. 2014, in Protostars and Planets VI, ed. H. Beuther, R. S. Klessen, C. P. Dullemond, & T. Henning, 387, doi: 10.2458/azu_uapress_9780816531240-ch017

Bai, X.-N., & Stone, J. M. 2011, , 736, 144, doi: 10.1088/0004-637X/736/2/144

Bailer-Jones, C. A. L., Rybizki, J., Fouesneau, M., Mantelet, G., & Andrae, R. 2018, , 156, 58, doi: 10.3847/1538-3881/aacb21

Balbus, S. A., & Hawley, J. F. 1991, , 376, 214, doi: 10.1086/170270

Banzatti, A., Pascucci, I., Bosman, A. D., et al. 2020, , 903, 124, doi: 10.3847/1538-4357/abbc1a

Banzatti, A., Abernathy, K. M., Brittain, S., et al. 2022, , 163, 174, doi: 10.3847/1538-3881/ac52f0

Basalgète, R., Ocaña, A. J., Féraud, G., et al. 2021, , 922, 213, doi: 10.3847/1538-4357/ac2d93

Bell, K. R., & Lin, D. N. C. 1994, , 427, 987, doi: 10.1086/174206

Benisty, M., Natta, A., Isella, A., et al. 2010, , 511, A74, doi: 10.1051/0004-6361/200912898

Bergin, E. A., & Cleeves, L. I. 2018, Chemistry During the Gas-Rich Stage of Planet Formation, 137, doi: 10.1007/978-3-319-55333-7_137

Bergin, E. A., Cleeves, L. I., Crockett, N., & Blake, G. A. 2014, Faraday Discussions, 168, 61, doi: 10.1039/C4FD00003J

Bergin, E. A., & Williams, J. P. 2017, Astrophysics and Space Science Library, Vol. 445, The Determination of Protoplanetary Disk Masses, ed. M. Pessah & O. Gressel, 1, doi: 10.1007/978-3-319-60609-5_1

Bergin, E. A., Cleeves, L. I., Gorti, U., et al. 2013, , 493, 644, doi: 10.1038/nature11805

Bergner, J. B., & Ciesla, F. 2021, , 919, 45, doi: 10.3847/1538-4357/ac0fd7

Bergner, J. B., Guzmán, V. G., Öberg, K. I., Loomis, R. A., & Pegues, J. 2018, , 857, 69, doi: 10.3847/1538-4357/aab664

Bergner, J. B., Öberg, K. I., Bergin, E. A., et al. 2019, , 876, 25, doi: 10.3847/1538-4357/ab141e

Bergner, J. B., Rajappan, M., & Öberg, K. I. 2022, , 933, 206, doi: 10.3847/1538-4357/ac771e

Bergner, J. B., Öberg, K. I., Bergin, E. A., et al. 2020, , 898, 97, doi: 10.3847/1538-4357/ab9e71

Bergner, J. B., Öberg, K. I., Guzmán, V. V., et al. 2021, , 257, 11, doi: 10.3847/1538-4365/ac143a

Bethell, T., & Bergin, E. 2009, Science, 326, 1675, doi: 10.1126/science.1176879

Bethell, T. J., & Bergin, E. A. 2011, , 739, 78, doi: 10.1088/0004-637X/739/2/78

Birnstiel, T., Klahr, H., & Ercolano, B. 2012, , 539, A148, doi: 10.1051/0004-6361/201118136

Birnstiel, T., Dullemond, C. P., Zhu, Z., et al. 2018, , 869, L45, doi: 10.3847/2041-8213/aaf743

Bisschop, S. E., Fraser, H. J., Öberg, K. I., van Dishoeck, E. F., & Schlemmer, S. 2006, , 449, 1297, doi: 10.1051/0004-6361:20054051

Boley, A. C., Mejía, A. C., Durisen, R. H., et al. 2006, , 651, 517, doi: 10.1086/507478

Boneberg, D. M., Panić, O., Haworth, T. J., Clarke, C. J., & Min, M. 2016, , 461, 385, doi: 10.1093/mnras/stw1325

Bonnell, I., & Bastien, P. 1992, , 401, L31, doi: 10.1086/186663

Booth, A. S., & Ilee, J. D. 2020, , 493, L108, doi: 10.1093/mnrasl/slaa014

Booth, A. S., Walsh, C., Ilee, J. D., et al. 2019, , 882, L31, doi: 10.3847/2041-8213/ab3645

Booth, A. S., Tabone, B., Ilee, J. D., et al. 2021, , 257, 16, doi: 10.3847/1538-4365/ac1ad4

Bosman, A. D., Alarcón, F., Zhang, K., & Bergin, E. A. 2021a, , 910, 3, doi: 10.3847/1538-4357/abe127

Bosman, A. D., & Bergin, E. A. 2021, , 918, L10, doi: 10.3847/2041-8213/ac1db1

Bosman, A. D., Bergin, E. A., Calahan, J., & Duval, S. E. 2022a, , 930, L26, doi: 10.3847/2041-8213/ac66ce

Bosman, A. D., Bergin, E. A., Calahan, J. K., & Duval, S. E. 2022b, , 933, L40, doi: 10.3847/2041-8213/ac7d9f

Bosman, A. D., Bruderer, S., & van Dishoeck, E. F. 2017, , 601, A36, doi: 10.1051/0004-6361/201629946

Bosman, A. D., Cridland, A. J., & Miguel, Y. 2019, , 632, L11, doi: 10.1051/0004-6361/201936827

Bosman, A. D., Walsh, C., & van Dishoeck, E. F. 2018a, , 618, A182, doi: 10.1051/0004-6361/201833497

—. 2018b, , 618, A182, doi: 10.1051/0004-6361/201833497

Bosman, A. D., Alarcón, F., Bergin, E. A., et al. 2021b, , 257, 7, doi: 10.3847/1538-4365/ac1435

—. 2021c, , 257, 7, doi: 10.3847/1538-4365/ac1435

Brewer, J. M., Fischer, D. A., & Madhusudhan, N. 2017, , 153, 83, doi: 10.3847/1538-3881/153/2/83

Brickhouse, N. S., Cranmer, S. R., Dupree, A. K., Luna, G. J. M., & Wolk, S. 2010, , 710, 1835, doi: 10.1088/0004-637X/710/2/1835

Brittain, S. D., Rettig, T. W., Simon, T., & Kulesa, C. 2005, , 626, 283, doi: 10.1086/429310

Bruderer, S. 2013, , 559, A46, doi: 10.1051/0004-6361/201321171

Bruderer, S., Doty, S. D., & Benz, A. O. 2009, , 183, 179, doi: 10.1088/0067-0049/183/2/179

Bruderer, S., van Dishoeck, E. F., Doty, S. D., & Herczeg, G. J. 2012, , 541, A91, doi: 10.1051/0004-6361/201118218

Calahan, J. K., Bergin, E. A., & Bosman, A. D. 2022, , 934, L14, doi: 10.3847/2041-8213/ac7e55

Calahan, J. K., Shirley, Y. L., Svoboda, B. E., et al. 2018, , 862, 63, doi: 10.3847/1538-4357/aabfea

Calahan, J. K., Bergin, E., Zhang, K., et al. 2021a, , 908, 8, doi: 10.3847/1538-4357/abd255

Calahan, J. K., Bergin, E. A., Zhang, K., et al. 2021b, , 257, 17, doi: 10.3847/1538-4365/ac143f

Calahan, J. K., Bergin, E., Zhang, K., et al. 2021c, , 908, 8, doi: 10.3847/1538-4357/abd255

Calahan, J. K., Bergin, E. A., Bosman, A. D., et al. 2023, Nature Astronomy, 7, 49, doi: 10.1038/s41550-022-01831-8

Calvet, N., D'Alessio, P., Hartmann, L., et al. 2002, , 568, 1008, doi: 10.1086/339061

Canta, A., Teague, R., Le Gal, R., & Öberg, K. I. 2021, , 922, 62, doi: 10.3847/1538-4357/ac23da

Carr, J. S., & Najita, J. R. 2008, Science, 319, 1504, doi: 10.1126/science.1153807

Carr, J. S., Najita, J. R., & Salyk, C. 2018, Research Notes of the American Astronomical Society, 2, 169, doi: 10.3847/2515-5172/aadfe7

Cassen, P., & Moosman, A. 1981, , 48, 353, doi: 10.1016/0019-1035(81)90051-8

Chandrasekhar, S. 1960, Proceedings of the National Academy of Science, 46, 253, doi: 10.1073/pnas.46.2.253

Chapillon, E., Dutrey, A., Guilloteau, S., et al. 2012, , 756, 58, doi: 10.1088/0004-637X/756/1/58

Ciesla, F. J., & Cuzzi, J. N. 2006, , 181, 178, doi: 10.1016/j.icarus.2005.11.009

Cieza, L. A., Casassus, S., Tobin, J., et al. 2016, , 535, 258, doi: 10.1038/nature18612

Cieza, L. A., Ruíz-Rodríguez, D., Perez, S., et al. 2018, , 474, 4347, doi: 10.1093/mnras/stx3059

Clayton, R. N. 1993, Annual Review of Earth and Planetary Sciences, 21, 115, doi: 10.1146/annurev.ea.21.050193.000555

Clayton, R. N., Grossman, L., & Mayeda, T. K. 1973, Science, 182, 485, doi: 10.1126/science.182.4111.485

Cleeves, L. I., Bergin, E. A., Qi, C., Adams, F. C., & Öberg, K. I. 2015, The Astrophysical Journal, 799, 204, doi: 10.1088/0004-637X/799/2/204

Cleeves, L. I., Öberg, K. I., Wilner, D. J., et al. 2018, , 865, 155, doi: 10.3847/1538-4357/aade96

Cleeves, L. I., Loomis, R. A., Teague, R., et al. 2021, , 911, 29, doi: 10.3847/1538-4357/abe862

Connelley, M. S., & Reipurth, B. 2018, , 861, 145, doi: 10.3847/1538-4357/aaba7b

Corazzi, M. A., Brucato, J. R., Poggiali, G., et al. 2021, , 913, 128, doi: 10.3847/1538-4357/abf6d3

Cridland, A. J., Bosman, A. D., & van Dishoeck, E. F. 2020, , 635, A68, doi: 10.1051/0004-6361/201936858

Cutri, R. M., Skrutskie, M. F., van Dyk, S., et al. 2003, 2MASS All Sky Catalog of point sources.

Czekala, I., Loomis, R. A., Teague, R., et al. 2021, arXiv e-prints, arXiv:2109.06188. https://arxiv.org/abs/2109.06188

D'Alessio, P., Calvet, N., Hartmann, L., Franco-Hernández, R., & Servín, H. 2006, , 638, 314, doi: 10.1086/498861

D'Alessio, P., Calvet, N., & Woolum, D. S. 2005, in Astronomical Society of the Pacific Conference Series, Vol. 341, Chondrites and the Protoplanetary Disk, ed. A. N. Krot, E. R. D. Scott, & B. Reipurth, 353

de Gregorio-Monsalvo, I., Ménard, F., Dent, W., et al. 2013, , 557, A133, doi: 10.1051/0004-6361/201321603

Debes, J. H., Jang-Condell, H., Weinberger, A. J., Roberge, A., & Schneider, G. 2013, , 771, 45, doi: 10.1088/0004-637X/771/1/45

Dent, W. R. F., Pinte, C., Cortes, P. C., et al. 2019, , 482, L29, doi: 10.1093/mnrasl/sly181

Draine, B. T. 2003, , 41, 241, doi: 10.1146/annurev.astro.41.011802.094840

Draine, B. T., & Lee, H. M. 1984, , 285, 89, doi: 10.1086/162480

Draine, B. T., & Li, A. 2001, , 551, 807, doi: 10.1086/320227

Draine, B. T., Roberge, W. G., & Dalgarno, A. 1983, , 264, 485, doi: 10.1086/160617

Du, F., & Bergin, E. A. 2014, , 792, 2, doi: 10.1088/0004-637X/792/1/2

Du, F., Bergin, E. A., & Hogerheijde, M. R. 2015, , 807, L32, doi: 10.1088/2041-8205/807/2/L32

Du, F., Bergin, E. A., Hogerheijde, M., et al. 2017, , 842, 98, doi: 10.3847/1538-4357/aa70ee

Dullemond, C. P., & Dominik, C. 2004, , 421, 1075, doi: 10.1051/0004-6361:20040284

Dullemond, C. P., Juhasz, A., Pohl, A., et al. 2012a, RADMC-3D: A multi-purpose radiative transfer tool. http://ascl.net/1202.015

—. 2012b, RADMC-3D: A multi-purpose radiative transfer tool, Astrophysics Source Code Library. http://ascl.net/1202.015

Eistrup, C., Walsh, C., & van Dishoeck, E. F. 2018, , 613, A14, doi: 10.1051/0004-6361/201731302

Facchini, S., Pinilla, P., van Dishoeck, E. F., & de Juan Ovelar, M. 2018, , 612, A104, doi: 10.1051/0004-6361/201731390

Fairlamb, J. R., Oudmaijer, R. D., Mendigutía, I., Ilee, J. D., & van den Ancker, M. E. 2015, , 453, 976, doi: 10.1093/mnras/stv1576

Faure, A., & Josselin, E. 2008, , 492, 257, doi: 10.1051/0004-6361:200810717

Favre, C., Cleeves, L. I., Bergin, E. A., Qi, C., & Blake, G. A. 2013, The Astrophysical Journal, 776, L38, doi: 10.1088/2041-8205/776/2/L38

Fayolle, E. C., Balfe, J., Loomis, R., et al. 2016, , 816, L28, doi: 10.3847/2041-8205/816/2/L28

Fedele, D., van Dishoeck, E. F., Kama, M., Bruderer, S., & Hogerheijde, M. R. 2016, , 591, A95, doi: 10.1051/0004-6361/201526948

Fehér, O., Kóspál, Á., Ábrahám, P., Hogerheijde, M. R., & Brinch, C. 2017, , 607, A39, doi: 10.1051/0004-6361/201731446

Flaherty, K. M., Hughes, A. M., Rosenfeld, K. A., et al. 2015, , 813, 99, doi: 10.1088/0004-637X/813/2/99

Flaherty, K. M., Hughes, A. M., Rose, S. C., et al. 2017, , 843, 150, doi: 10.3847/1538-4357/aa79f9

Flock, M., Henning, T., & Klahr, H. 2012, , 761, 95, doi: 10.1088/0004-637X/761/2/95

Folsom, C. P., Bagnulo, S., Wade, G. A., et al. 2012, , 422, 2072, doi: 10.1111/j.1365-2966.2012.20718.x

Fraser, H. J., Collings, M. P., McCoustra, M. R. S., & Williams, D. A. 2001, , 327, 1165, doi: 10.1046/j.1365-8711.2001.04835.x

Frerking, M. A., Langer, W. D., & Wilson, R. W. 1982, , 262, 590, doi: 10.1086/160451

Fuchs, G. W., Cuppen, H. M., Ioppolo, S., et al. 2009, , 505, 629, doi: 10.1051/0004-6361/200810784

Gaia Collaboration, Brown, A. G. A., Vallenari, A., et al. 2020, arXiv e-prints, arXiv:2012.01533. https://arxiv.org/abs/2012.01533

—. 2018, , 616, A1, doi: 10.1051/0004-6361/201833051

Gammie, C. F., & Ostriker, E. C. 1996, , 466, 814, doi: 10.1086/177556

Garrod, R. T., Widicus Weaver, S. L., & Herbst, E. 2008, , 682, 283, doi: 10.1086/588035

Garufi, A., Quanz, S. P., Schmid, H. M., et al. 2014, , 568, A40, doi: 10.1051/0004-6361/201424262

Glassgold, A. E., Najita, J., & Igea, J. 2004, , 615, 972, doi: 10.1086/424509

Goldsmith, P. F., & Langer, W. D. 1999, , 517, 209, doi: 10.1086/307195

Gordon, I. E., Rothman, L. S., Hargreaves, R. J., et al. 2022, , 277, 107949, doi: 10.1016/j.jqsrt.2021.107949

Gorti, U., Hollenbach, D., Najita, J., & Pascucci, I. 2011, , 735, 90, doi: 10.1088/0004-637X/735/2/90

Goumans, T. P. M., Uppal, M. A., & Brown, W. A. 2008, , 384, 1158, doi: 10.1111/j.1365-2966.2007.12788.x

Grady, C. A., Devine, D., Woodgate, B., et al. 2000, , 544, 895, doi: 10.1086/317222

Green, J. D., Evans, Neal J., I., Kóspál, Á., et al. 2013, , 772, 117, doi: 10.1088/0004-637X/772/2/117

Gressel, O., Nelson, R. P., & Turner, N. J. 2012, , 422, 1140, doi: 10.1111/j.1365-2966.2012.20701.x

Gundlach, B., & Blum, J. 2015, , 798, 34, doi: 10.1088/0004-637X/798/1/34

Guzmán, V. V., Bergner, J. B., Law, C. J., et al. 2021, , 257, 6, doi: 10.3847/1538-4365/ac1440

Haisch, Karl E., J., Lada, E. A., & Lada, C. J. 2001, , 553, L153, doi: 10.1086/320685

Harries, T. J., Haworth, T. J., Acreman, D., Ali, A., & Douglas, T. 2019, Astronomy and Computing, 27, 63, doi: 10.1016/j.ascom.2019.03.002

Harries, T. J., Monnier, J. D., Symington, N. H., & K̂urosawa, R. 2004, mnras, 350, 565, doi: 10.1111/j.1365-2966.2004.07668.x

Hartmann, L., Calvet, N., Gullbring, E., & D'Alessio, P. 1998, , 495, 385, doi: 10.1086/305277

Hartmann, L., & Kenyon, S. J. 1996, , 34, 207, doi: 10.1146/annurev.astro.34.1.207

Hartmann, L., Megeath, S. T., Allen, L., et al. 2005, , 629, 881, doi: 10.1086/431472

Hasegawa, T. I., Herbst, E., & Leung, C. M. 1992, , 82, 167, doi: 10.1086/191713

Hawley, J. F., & Stone, J. M. 1998, , 501, 758, doi: 10.1086/305849

Hayashi, C. 1981, Progress of Theoretical Physics Supplement, 70, 35, doi: 10.1143/PTPS.70.35

Heays, A. N., Bosman, A. D., & van Dishoeck, E. F. 2017, , 602, A105, doi: 10.1051/0004-6361/201628742

Henning, T., & Stognienko, R. 1996, , 311, 291

Herczeg, G. J., Linsky, J. L., Valenti, J. A., Johns-Krull, C. M., & Wood, B. E. 2002, , 572, 310, doi: 10.1086/339731

Hernández, J., Hartmann, L., Calvet, N., et al. 2008, , 686, 1195, doi: 10.1086/591224

Hernández, J., Hartmann, L., Megeath, T., et al. 2007, , 662, 1067, doi: 10.1086/513735

Hillenbrand, L. A., Miller, A. A., Covey, K. R., et al. 2013, , 145, 59, doi: 10.1088/0004-6256/145/3/59

Houck, J. R., Roellig, T. L., Van Cleve, J., et al. 2004, in Society of Photo-Optical Instrumentation Engineers (SPIE) Conference Series, Vol. 5487, Optical, Infrared, and Millimeter Space Telescopes, ed. J. C. Mather, 62–76, doi: 10.1117/12.550517

Huang, J., Andrews, S. M., Cleeves, L. I., et al. 2018, , 852, 122, doi: 10.3847/1538-4357/aaa1e7

Ibryamov, S. I., Semkov, E. H., & Peneva, S. P. 2018, , 35, e007, doi: 10.1017/pasa.2018.2

Ilee, J. D., Walsh, C., Booth, A. S., et al. 2021, , 257, 9, doi: 10.3847/1538-4365/ac1441

Ioppolo, S., Cuppen, H. M., Romanzin, C., van Dishoeck, E. F., & Linnartz, H. 2008, , 686, 1474, doi: 10.1086/591506

—. 2010, Physical Chemistry Chemical Physics (Incorporating Faraday Transactions), 12, 12065, doi: 10.1039/C0CP00250J

Isella, A., Testi, L., Natta, A., et al. 2007, , 469, 213, doi: 10.1051/0004-6361:20077385

Isella, A., Huang, J., Andrews, S. M., et al. 2018, , 869, L49, doi: 10.3847/2041-8213/aaf747

Jang-Condell, H. 2008, , 679, 797, doi: 10.1086/533583

Johansen, A., & Lambrechts, M. 2017, Annual Review of Earth and Planetary Sciences, 45, 359, doi: 10.1146/annurev-earth-063016-020226

Johnson, J. A., Aller, K. M., Howard, A. W., & Crepp, J. R. 2010, , 122, 905, doi: 10.1086/655775

Jorsater, S., & van Moorsel, G. A. 1995, , 110, 2037, doi: 10.1086/117668

Kama, M., Bruderer, S., van Dishoeck, E. F., et al. 2016a, , 592, A83, doi: 10.1051/0004-6361/201526991

—. 2016b, , 592, A83, doi: 10.1051/0004-6361/201526991

Kama, M., Trapman, L., Fedele, D., et al. 2020a, , 634, A88, doi: 10.1051/0004-6361/201937124

—. 2020b, , 634, A88, doi: 10.1051/0004-6361/201937124

Kamp, I., & Dullemond, C. P. 2004, , 615, 991, doi: 10.1086/424703

Kamp, I., Tilling, I., Woitke, P., Thi, W. F., & Hogerheijde, M. 2010, , 510, A18, doi: 10.1051/0004-6361/200913076

Kanagawa, K. D., Muto, T., Tanaka, H., et al. 2015, , 806, L15, doi: 10.1088/2041-8205/806/1/L15

Kastner, J. H., Qi, C., Dickson-Vandervelde, D. A., et al. 2018, , 863, 106, doi: 10.3847/1538-4357/aacff7

Kenyon, S. J., & Hartmann, L. 1987, , 323, 714, doi: 10.1086/165866

—. 1995, , 101, 117, doi: 10.1086/192235

Koerner, D. W., Sargent, A. I., & Ostroff, N. A. 2001, , 560, L181, doi: 10.1086/324226

Kóspál, Á., Ábrahám, P., Acosta-Pulido, J. A., et al. 2013, , 551, A62, doi: 10.1051/0004-6361/201220553

Krijt, S., Ormel, C. W., Dominik, C., & Tielens, A. G. G. M. 2016, , 586, A20, doi: 10.1051/0004-6361/201527533

Krijt, S., Schwarz, K. R., Bergin, E. A., & Ciesla, F. J. 2018, , 864, 78, doi: 10.3847/1538-4357/aad69b

Kruijer, T. S., Burkhardt, C., Budde, G., & Kleine, T. 2017, Proceedings of the National Academy of Science, 114, 6712, doi: 10.1073/pnas.1704461114

Kuznetsova, A., Bae, J., Hartmann, L., & Mac Low, M.-M. 2022, , 928, 92, doi: 10.3847/1538-4357/ac54a8

Lacy, J. H., Knacke, R., Geballe, T. R., & Tokunaga, A. T. 1994, , 428, L69, doi: 10.1086/187395

Lacy, J. H., Sneden, C., Kim, H., & Jaffe, D. T. 2017, , 838, 66, doi: 10.3847/1538-4357/aa6247

Lada, C. J. 1987, in Star Forming Regions, ed. M. Peimbert & J. Jugaku, Vol. 115, 1

Lambrechts, M., Johansen, A., & Morbidelli, A. 2014, , 572, A35, doi: 10.1051/0004-6361/201423814

Law, C. J., Teague, R., Loomis, R. A., et al. 2021a, arXiv e-prints, arXiv:2109.06217. https://arxiv.org/abs/2109.06217

Law, C. J., Loomis, R. A., Teague, R., et al. 2021b, , 257, 3, doi: 10.3847/1538-4365/ac1434

—. 2021c, arXiv e-prints, arXiv:2109.06210. https://arxiv.org/abs/2109.06210

Law, C. J., Teague, R., Loomis, R. A., et al. 2021d, , 257, 4, doi: 10.3847/1538-4365/ac1439

Law, C. J., Crystian, S., Teague, R., et al. 2022, , 932, 114, doi: 10.3847/1538-4357/ac6c02

Le Gal, R., Brady, M. T., Öberg, K. I., Roueff, E., & Le Petit, F. 2019, , 886, 86, doi: 10.3847/1538-4357/ab4ad9

Lee, J.-E., Bergin, E. A., & Lyons, J. R. 2008, , 43, 1351, doi: 10.1111/j.1945-5100.2008.tb00702.x

Li, A., & Draine, B. T. 2001, , 554, 778, doi: 10.1086/323147

Linsky, J. L. 1998, , 84, 285

Linsky, J. L., Draine, B. T., Moos, H. W., et al. 2006, , 647, 1106, doi: 10.1086/505556

Liu, H. B., Galván-Madrid, R., Vorobyov, E. I., et al. 2016, , 816, L29, doi: 10.3847/2041-8205/816/2/L29

Liu, H. B., Dunham, M. M., Pascucci, I., et al. 2018, , 612, A54, doi: 10.1051/0004-6361/201731951

Long, F., Herczeg, G. J., Pascucci, I., et al. 2017, , 844, 99, doi: 10.3847/1538-4357/aa78fc

Loomis, R. A., Cleeves, L. I., Öberg, K. I., et al. 2018, , 859, 131, doi: 10.3847/1538-4357/aac169

Low, F. J., Smith, P. S., Werner, M., et al. 2005, , 631, 1170, doi: 10.1086/432640

Lucy, L. B. 1999, , 344, 282

Lynden-Bell, D., & Pringle, J. E. 1974, , 168, 603, doi: 10.1093/mnras/168.3.603

Lyons, J. R., & Young, E. D. 2005, , 435, 317, doi: 10.1038/nature03557

Madhusudhan, N., Mousis, O., Johnson, T. V., & Lunine, J. I. 2011, , 743, 191, doi: 10.1088/0004-637X/743/2/191

Manara, C. F., Morbidelli, A., & Guillot, T. 2018, , 618, L3, doi: 10.1051/0004-6361/201834076

Mangum, J. G., & Shirley, Y. L. 2015, , 127, 266, doi: 10.1086/680323

Mann, R. K., & Williams, J. P. 2010, , 725, 430, doi: 10.1088/0004-637X/725/1/430

Mathis, J. S., Rumpl, W., & Nordsieck, K. H. 1977, , 217, 425, doi: 10.1086/155591

McClure, M. K., Bergin, E. A., Cleeves, L. I., et al. 2016, , 831, 167, doi: 10.3847/0004-637X/831/2/167

McClure, M. K., Rocha, W. R. M., Pontoppidan, K. M., et al. 2023, Nature Astronomy, 7, 431, doi: 10.1038/s41550-022-01875-w

McElroy, D., Walsh, C., Markwick, A. J., et al. 2013, , 550, A36, doi: 10.1051/0004-6361/201220465

McKee, C. F., & Ostriker, E. C. 2007, , 45, 565, doi: 10.1146/annurev.astro.45.051806.110602

McMullin, J. P., Waters, B., Schiebel, D., Young, W., & Golap, K. 2007, in Astronomical Society of the Pacific Conference Series, Vol. 376, Astronomical Data Analysis Software and Systems XVI, ed. R. A. Shaw, F. Hill, & D. J. Bell, 127

Meijerink, R., Pontoppidan, K. M., Blake, G. A., Poelman, D. R., & Dullemond, C. P. 2009, , 704, 1471, doi: 10.1088/0004-637X/704/2/1471

Mekkaden, M. V. 1998, , 340, 135

Miotello, A., Bruderer, S., & van Dishoeck, E. F. 2014, , 572, A96, doi: 10.1051/0004-6361/201424712

Miotello, A., Kamp, I., Birnstiel, T., Cleeves, L. I., & Kataoka, A. 2022, arXiv e-prints, arXiv:2203.09818. https://arxiv.org/abs/2203.09818

Miotello, A., van Dishoeck, E. F., Kama, M., & Bruderer, S. 2016, , 594, A85, doi: 10.1051/0004-6361/201628159

Miotello, A., van Dishoeck, E. F., Williams, J. P., et al. 2017, , 599, A113, doi: 10.1051/0004-6361/201629556

Miotello, A., Facchini, S., van Dishoeck, E. F., et al. 2019, , 631, A69, doi: 10.1051/0004-6361/201935441

Molyarova, T., Akimkin, V., Semenov, D., et al. 2018, , 866, 46, doi: 10.3847/1538-4357/aadfd9

Monnier, J. D., Harries, T. J., Aarnio, A., et al. 2017, , 838, 20, doi: 10.3847/1538-4357/aa6248

Mulders, G. D., Pascucci, I., Apai, D., & Ciesla, F. J. 2018, , 156, 24, doi: 10.3847/1538-3881/aac5ea

Müller, H. S. P., Schlöder, F., Stutzki, J., & Winnewisser, G. 2005, Journal of Molecular Structure, 742, 215, doi: 10.1016/j.molstruc.2005.01.027

Müller, H. S. P., Thorwirth, S., Roth, D. A., & Winnewisser, G. 2001, , 370, L49, doi: 10.1051/0004-6361:20010367

Muro-Arena, G. A., Dominik, C., Waters, L. B. F. M., et al. 2018, , 614, A24, doi: 10.1051/0004-6361/201732299

Najita, J. R., & Ádámkovics, M. 2017, , 847, 6, doi: 10.3847/1538-4357/aa8632

Najita, J. R., Ádámkovics, M., & Glassgold, A. E. 2011, , 743, 147, doi: 10.1088/0004-637X/743/2/147

Nazari, P., Meijerhof, J. D., van Gelder, M. L., et al. 2022, , 668, A109, doi: 10.1051/0004-6361/202243788

Nealon, R., Pinte, C., Alexander, R., Mentiplay, D., & Dipierro, G. 2019, , 484, 4951, doi: 10.1093/mnras/stz346

Nittler, L. R., & Gaidos, E. 2012, , 47, 2031, doi: 10.1111/j.1945-5100.2012.01410.x

Nomura, H., Aikawa, Y., Tsujimoto, M., Nakagawa, Y., & Millar, T. J. 2007, , 661, 334, doi: 10.1086/513419

Nomura, H., & Millar, T. J. 2005, , 438, 923, doi: 10.1051/0004-6361:20052809

Oba, Y., Watanabe, N., Hama, T., et al. 2012, , 749, 67, doi: 10.1088/0004-637X/749/1/67

Öberg, K. I., & Bergin, E. A. 2016, , 831, L19, doi: 10.3847/2041-8205/831/2/L19

Öberg, K. I., Boogert, A. C. A., Pontoppidan, K. M., et al. 2011a, , 740, 109, doi: 10.1088/0004-637X/740/2/109

Öberg, K. I., Guzmán, V. V., Furuya, K., et al. 2015, , 520, 198, doi: 10.1038/nature14276

Öberg, K. I., Murray-Clay, R., & Bergin, E. A. 2011b, , 743, L16, doi: 10.1088/2041-8205/743/1/L16

Öberg, K. I., & Wordsworth, R. 2019, , 158, 194, doi: 10.3847/1538-3881/ab46a8

Öberg, K. I., Guzmán, V. V., Walsh, C., et al. 2021, , 257, 1, doi: 10.3847/1538-4365/ac1432

Oberg, K. I., Guzman, V. V., Walsh, C., et al. 2021, arXiv e-prints, arXiv:2109.06268. https://arxiv.org/abs/2109.06268

Okuzumi, S., Momose, M., Sirono, S.-i., Kobayashi, H., & Tanaka, H. 2016, , 821, 82, doi: 10.3847/0004-637X/821/2/82

Penna, R. F., Sądowski, A., Kulkarni, A. K., & Narayan, R. 2013, , 428, 2255, doi: 10.1093/mnras/sts185

Perez-Becker, D., & Chiang, E. 2011, , 735, 8, doi: 10.1088/0004-637X/735/1/8

Pickett, H. M., Poynter, R. L., Cohen, E. A., et al. 1998, , 60, 883, doi: 10.1016/S0022-4073(98)00091-0

Pilbratt, G. L., Riedinger, J. R., Passvogel, T., et al. 2010, , 518, L1, doi: 10.1051/0004-6361/201014759

Pineda, J. E., Segura-Cox, D., Caselli, P., et al. 2020, Nature Astronomy, 4, 1158, doi: 10.1038/s41550-020-1150-z

Pinte, C., Harries, T. J., Min, M., et al. 2009, , 498, 967, doi: 10.1051/0004-6361/200811555

Pinte, C., Price, D. J., Ménard, F., et al. 2018a, , 860, L13, doi: 10.3847/2041-8213/aac6dc

—. 2018b, , 860, L13, doi: 10.3847/2041-8213/aac6dc

—. 2020, , 890, L9, doi: 10.3847/2041-8213/ab6dda

Poglitsch, A., Waelkens, C., Geis, N., et al. 2010, , 518, L2, doi: 10.1051/0004-6361/201014535

Pontoppidan, K. M., Salyk, C., Bergin, E. A., et al. 2014, in Protostars and Planets VI, ed. H. Beuther, R. S. Klessen, C. P. Dullemond, & T. Henning, 363, doi: 10.2458/azu_uapress_9780816531240-ch016

Pontoppidan, K. M., Salyk, C., Blake, G. A., et al. 2010, , 720, 887, doi: 10.1088/0004-637X/720/1/887

Postel, A., Audard, M., Vorobyov, E., et al. 2019, , 631, A30, doi: 10.1051/0004-6361/201935601

Powell, D., Murray-Clay, R., Pérez, L. M., Schlichting, H. E., & Rosenthal, M. 2019, , 878, 116, doi: 10.3847/1538-4357/ab20ce

Powner, M. W., Gerland, B., & Sutherland, J. D. 2009, , 459, 239, doi: 10.1038/nature08013

Principe, D. A., Cieza, L., Hales, A., et al. 2018, , 473, 879, doi: 10.1093/mnras/stx2320

Qi, C., D'Alessio, P., Öberg, K. I., et al. 2011, , 740, 84, doi: 10.1088/0004-637X/740/2/84

Qi, C., Öberg, K. I., Andrews, S. M., et al. 2015, , 813, 128, doi: 10.1088/0004-637X/813/2/128

Qi, C., Ho, P. T. P., Wilner, D. J., et al. 2004, , 616, L11, doi: 10.1086/421063

Quanz, S. P., Henning, T., Bouwman, J., et al. 2007, , 668, 359, doi: 10.1086/521219

Rab, C., Kamp, I., Dominik, C., et al. 2020, arXiv e-prints, arXiv:2008.05941. https://arxiv.org/abs/2008.05941

Reboussin, L., Wakelam, V., Guilloteau, S., Hersant, F., & Dutrey, A. 2015, , 579, A82, doi: 10.1051/0004-6361/201525885

Rich, E. A., Wisniewski, J. P., Sitko, M. L., et al. 2020, , 902, 4, doi: 10.3847/1538-4357/abb2a3

Richards, S. N., Moseley, S. H., Stacey, G., et al. 2018, Journal of Astronomical Instrumentation, 7, 1840015, doi: 10.1142/S2251171718400159

Rieke, G. H., Wright, G. S., Böker, T., et al. 2015, , 127, 584, doi: 10.1086/682252

Ritson, D., & Sutherland, J. D. 2012, Nature Chemistry, 4, 895, doi: 10.1038/nchem.1467

Röllig, M., & Ossenkopf, V. 2013, , 550, A56, doi: 10.1051/0004-6361/201220130

Rosenfeld, K. A., Andrews, S. M., Hughes, A. M., Wilner, D. J., & Qi, C. 2013, , 774, 16, doi: 10.1088/0004-637X/774/1/16

Rothman, L. S., Jacquemart, D., Barbe, A., et al. 2005, , 96, 139, doi: 10.1016/j.jqsrt.2004.10.008

Ruffle, D. P., & Herbst, E. 2001, , 324, 1054, doi: 10.1046/j.1365-8711.2001.04394.x

Salyk, C., Pontoppidan, K. M., Blake, G. A., Najita, J. R., & Carr, J. S. 2011a, , 731, 130, doi: 10.1088/0004-637X/731/2/130

—. 2011b, , 731, 130, doi: 10.1088/0004-637X/731/2/130

Schindhelm, R., France, K., Herczeg, G. J., et al. 2012, , 756, L23, doi: 10.1088/2041-8205/756/1/L23

Schöier, F. L., van der Tak, F. F. S., van Dishoeck, E. F., & Black, J. H. 2005, , 432, 369, doi: 10.1051/0004-6361:20041729

Schoonenberg, D., & Ormel, C. W. 2017, , 602, A21, doi: 10.1051/0004-6361/201630013

Schwarz, K. R., Bergin, E. A., Cleeves, L. I., et al. 2016, , 823, 91, doi: 10.3847/0004-637X/823/2/91

—. 2018, , 856, 85, doi: 10.3847/1538-4357/aaae08

—. 2019, , 877, 131, doi: 10.3847/1538-4357/ab1c5e

Seok, J. Y., & Li, A. 2017, , 835, 291, doi: 10.3847/1538-4357/835/2/291

Shakura, N. I., & Sunyaev, R. A. 1973, , 500, 33

Sloan, G. C., Kraemer, K. E., Price, S. D., & Shipman, R. F. 2003, , 147, 379, doi: 10.1086/375443

Smith, R. L., Pontoppidan, K. M., Young, E. D., & Morris, M. R. 2015, , 813, 120, doi: 10.1088/0004-637X/813/2/120

Smith, R. L., Pontoppidan, K. M., Young, E. D., Morris, M. R., & van Dishoeck, E. F. 2009, , 701, 163, doi: 10.1088/0004-637X/701/1/163

Stevenson, D. J., & Lunine, J. I. 1988, , 75, 146, doi: 10.1016/0019-1035(88)90133-9

Stolker, T., Dominik, C., Min, M., et al. 2016, , 596, A70, doi: 10.1051/0004-6361/201629098

Sutherland, J. D. 2015, Angewandte Chemie, 55, 104, doi: 10.1002/anie.201506585

Teague, R. 2019, The Journal of Open Source Software, 4, 1632, doi: 10.21105/joss.01632

Teague, R., Bae, J., & Bergin, E. A. 2019a, , 574, 378, doi: 10.1038/s41586-019-1642-0

—. 2019b, , 574, 378, doi: 10.1038/s41586-019-1642-0

Teague, R., & Foreman-Mackey, D. 2018, Research Notes of the American Astronomical Society, 2, 173, doi: 10.3847/2515-5172/aae265

Teague, R., Law, C. J., Huang, J., & Meng, F. 2021, Journal of Open Source Software, 6, 3827, doi: 10.21105/joss.03827

Teague, R., Bae, J., Aikawa, Y., et al. 2021, arXiv e-prints, arXiv:2109.06218. https://arxiv.org/abs/2109.06218

Thi, W. F., Mathews, G., Ménard, F., et al. 2010, , 518, L125, doi: 10.1051/0004-6361/201014578

Thiemens, M. H., & Heidenreich, J. E., I. 1983, Science, 219, 1073, doi: 10.1126/science.219.4588.1073

Tilling, I., Woitke, P., Meeus, G., et al. 2012, , 538, A20, doi: 10.1051/0004-6361/201116919

Tobin, J. J., van't Hoff, M. L. R., Leemker, M., et al. 2023, , 615, 227, doi: 10.1038/s41586-022-05676-z

Trapman, L., Miotello, A., Kama, M., van Dishoeck, E. F., & Bruderer, S. 2017, , 605, A69, doi: 10.1051/0004-6361/201630308

Trapman, L., Zhang, K., van't Hoff, M. L. R., Hogerheijde, M. R., & Bergin, E. A. 2022, , 926, L2, doi: 10.3847/2041-8213/ac4f47

van Boekel, R., Henning, T., Menu, J., et al. 2017, , 837, 132, doi: 10.3847/1538-4357/aa5d68

Van Clepper, E., Bergner, J. B., Bosman, A. D., Bergin, E., & Ciesla, F. J. 2022, , 927, 206, doi: 10.3847/1538-4357/ac511b

van der Marel, N., van Dishoeck, E. F., Bruderer, S., et al. 2016, , 585, A58, doi: 10.1051/0004-6361/201526988

van der Marel, N., Williams, J. P., & Bruderer, S. 2018, , 867, L14, doi: 10.3847/2041-8213/aae88e

van Dishoeck, E. F., & Black, J. H. 1988, , 334, 771, doi: 10.1086/166877

van Dishoeck, E. F., Jonkheid, B., & van Hemert, M. C. 2006, Faraday Discussions, 133, 231, doi: 10.1039/b517564j

van 't Hoff, M. L. R., Walsh, C., Kama, M., Facchini, S., & van Dishoeck, E. F. 2017, , 599, A101, doi: 10.1051/0004-6361/201629452

van Zadelhoff, G. J., van Dishoeck, E. F., Thi, W. F., & Blake, G. A. 2001, , 377, 566, doi: 10.1051/0004-6361:20011137

van't Hoff, M. L. R., Harsono, D., van Gelder, M. L., et al. 2022, , 924, 5, doi: 10.3847/1538-4357/ac3080

Vasyunin, A. I., & Herbst, E. 2013, , 769, 34, doi: 10.1088/0004-637X/769/1/34

Visser, R., Bergin, E. A., & Jørgensen, J. K. 2015, , 577, A102, doi: 10.1051/0004-6361/201425365

Visser, R., van Dishoeck, E. F., & Black, J. H. 2009, , 503, 323, doi: 10.1051/0004-6361/200912129

Vorobyov, E. I., & Basu, S. 2006, , 650, 956, doi: 10.1086/507320

—. 2015, , 805, 115, doi: 10.1088/0004-637X/805/2/115

Vorobyov, E. I., Zakhozhay, O. V., & Dunham, M. M. 2013, , 433, 3256, doi: 10.1093/mnras/stt970

Walsh, C., Millar, T. J., Nomura, H., et al. 2014, , 563, A33, doi: 10.1051/0004-6361/201322446

Walsh, C., Loomis, R. A., Öberg, K. I., et al. 2016, , 823, L10, doi: 10.3847/2041-8205/823/1/L10

Wang, H., Bell, R. C., Iedema, M. J., Tsekouras, A. A., & Cowin, J. P. 2005, , 620, 1027, doi: 10.1086/427072

Warren, S. G., & Brandt, R. E. 2008, Journal of Geophysical Research (Atmospheres), 113, D14220, doi: 10.1029/2007JD009744

Weaver, E., Isella, A., & Boehler, Y. 2018, , 853, 113, doi: 10.3847/1538-4357/aaa481

Weidenschilling, S. J. 1977, , 180, 57, doi: 10.1093/mnras/180.2.57

Weintraub, D. A., Masson, C. R., & Zuckerman, B. 1989a, , 344, 915, doi: 10.1086/167859

Weintraub, D. A., Sandell, G., & Duncan, W. D. 1989b, , 340, L69, doi: 10.1086/185441

Weintraub, D. A., Saumon, D., Kastner, J. H., & Forveille, T. 2000, , 530, 867, doi: 10.1086/308402

Wichittanakom, C., Oudmaijer, R. D., Fairlamb, J. R., et al. 2020, , 493, 234, doi: 10.1093/mnras/staa169

Williams, J. P., & Best, W. M. J. 2014, , 788, 59, doi: 10.1088/0004-637X/788/1/59

Williams, J. P., & Cieza, L. A. 2011, , 49, 67, doi: 10.1146/annurev-astro-081710-102548

Williams, J. P., & McPartland, C. 2016, , 830, 32, doi: 10.3847/0004-637X/830/1/32

Wilner, D. J., Bourke, T. L., Wright, C. M., et al. 2003, , 596, 597, doi: 10.1086/377627

Wilner, D. J., Ho, P. T. P., Kastner, J. H., & Rodríguez, L. F. 2000, , 534, L101, doi: 10.1086/312642

Wilson, T. L. 1999, Reports on Progress in Physics, 62, 143, doi: 10.1088/0034-4885/62/2/002

Wilson, T. L., & Rood, R. 1994, , 32, 191, doi: 10.1146/annurev.aa.32.090194.001203

Wisniewski, J. P., Clampin, M., Grady, C. A., et al. 2008, , 682, 548, doi: 10.1086/589629

Woitke, P., Kamp, I., & Thi, W. F. 2009, , 501, 383, doi: 10.1051/0004-6361/200911821

Woitke, P., Min, M., Pinte, C., et al. 2016, , 586, A103, doi: 10.1051/0004-6361/201526538

Woitke, P., Kamp, I., Antonellini, S., et al. 2019, , 131, 064301, doi: 10.1088/1538-3873/aaf4e5

Woodall, J., Agúndez, M., Markwick-Kemper, A. J., & Millar, T. J. 2007, , 466, 1197, doi: 10.1051/0004-6361:20064981

Woods, P. M., & Willacy, K. 2009, , 693, 1360, doi: 10.1088/0004-637X/693/2/1360

Wyatt, M. C., Panić, O., Kennedy, G. M., & Matrà, L. 2015, , 357, 103, doi: 10.1007/s10509-015-2315-6

Xie, C., Haffert, S. Y., de Boer, J., et al. 2021, , 650, L6, doi: 10.1051/0004-6361/202140602

Yurimoto, H., & Kuramoto, K. 2004, Science, 305, 1763, doi: 10.1126/science.1100989

Zhang, K., Bergin, E. A., Blake, G. A., Cleeves, L. I., & Schwarz, K. R. 2017, Nature Astronomy, 1, 0130, doi: 10.1038/s41550-017-0130

Zhang, K., Bergin, E. A., Schwarz, K., Krijt, S., & Ciesla, F. 2019, , 883, 98, doi: 10.3847/1538-4357/ab38b9

Zhang, K., Blake, G. A., & Bergin, E. A. 2015, , 806, L7, doi: 10.1088/2041-8205/806/1/L7

Zhang, K., Bosman, A. D., & Bergin, E. A. 2020a, , 891, L16, doi: 10.3847/2041-8213/ab77ca

—. 2020b, , 891, L16, doi: 10.3847/2041-8213/ab77ca

Zhang, K., Pontoppidan, K. M., Salyk, C., & Blake, G. A. 2013, , 766, 82, doi: 10.1088/0004-637X/766/2/82

Zhang, K., Schwarz, K. R., & Bergin, E. A. 2020c, , 891, L17, doi: 10.3847/2041-8213/ab7823

Zhang, K., Booth, A. S., Law, C. J., et al. 2021a, arXiv e-prints, arXiv:2109.06233. https://arxiv.org/abs/2109.06233

—. 2021b, arXiv e-prints, arXiv:2109.06233. https://arxiv.org/abs/2109.06233

Zhang, S., Zhu, Z., Huang, J., et al. 2018, , 869, L47, doi: 10.3847/2041-8213/aaf744

Zhang, Y., Snellen, I. A. G., Bohn, A. J., et al. 2021c, , 595, 370, doi: 10.1038/s41586-021-03616-x

Zhu, Z., Hartmann, L., Gammie, C., & McKinney, J. C. 2009, , 701, 620, doi: 10.1088/0004-637X/701/1/620

Zhu, Z., Zhang, S., Jiang, Y.-F., et al. 2019, , 877, L18, doi: 10.3847/2041-8213/ab1f8c